

Solving the transport equation by the use of 6D spectral methods in spherical coordinates

S. Bonazzola¹, N. Vassetz^{2,1} and B. Peres¹

¹ Laboratoire Univers et Théories, Observatoire de Paris, CNRS, Université Paris Diderot, 5 place Jules Janssen, F-92190, Meudon, France.

² Universitaet Basel, Departement Physik, Klingelbergstrasse 82, CH-4056 Basel, Switzerland.
e-mail: silvano.bonazzola@obspm.fr, nicolas.vasset@unibas.ch, bruno.peres@obspm.fr

6 June 2011 / 6 July 2011

ABSTRACT

We present a numerical method for handling the resolution of a general transport equation for radiative particles, aimed at physical problems with a doubly spherical geometry. Having in mind the computational time difficulties encountered in problems such as neutrino transport in astrophysical supernovae, we propose a scheme based on full spectral methods in 6d spherical coordinates. This approach, known to be suited when the characteristic length of the dynamics is much smaller than the domain size, has the potential advantage of a global speedup with respect to usual finite difference schemes. An analysis of the properties of the Liouville operator expressed in our coordinates is necessary in order to handle correctly the numerical behaviour of the solution. This reflects on a specific (spherical) geometry of the computational domain. The numerical tests, performed under several different regimes for the equation, prove the robustness of the scheme: their performances also point out to the suitability of such an approach to large scale computations involving transport physics for massless radiative particles. **We wish to point out that the algorithm presented here, is particularly suitable to treat problems in which matter has high velocities, such as the neutrino transport in supernovae.**

Key words. Transport equations – Radiative astrophysics – Spectral methods

1. Introduction

Particle transport phenomena are central in modelling systems governed by radiative hydrodynamics, encountered very often in astrophysics as well as in plasma physics. A global description of radiative transport involves the hyperbolic transport equation, sometimes called Boltzmann equation in the literature¹. This equation describes the time evolution of a distribution function F defined on a 6-dimensional phase space. The high dimensionality of this equation often prevents its numerical resolution in the most general geometry, due to unaffordable computational resources for obtaining physical results in a reasonable CPU time, when using classical techniques. As a result, most numerical models for radiative transport physics in several settings either restrict the global geometry of the problem (as in Mezzacappa & Matzner (1989); Gourgoulhon & Haensel (1993); Liebendörfer et al. (2005); Müller et al. (2010)), or replace the transport equation by simplified models usually involving the distribution moments (Anderson & Spiegel (1972); Levermore (1979); Thorne (1981); Cardall & Mezzacappa (2003); Liebendörfer et al. (2009)). However, in the particular setting of neutrino transport in astrophysical supernovae, the fact

that a multidimensional transport model for neutrino radiation is required to reproduce the observed supernova explosions has been strongly hinted in recent simulations (Liebendörfer et al. 2005). As a result, attempts have been made in this direction, but they result in very demanding simulations, that are still not able to capture all the needed physics in a general geometry (Messer et al. 2008; Marek & Janka 2009).

Apart from the problem of dimensionality and size of the simulations, transport phenomena very often involve physical processes occurring through several orders of magnitude for typical lengths. Once again, this problem arises in the supernovae neutrinos setting, when comparing the mean free path of a radiative particle in the diffusion regime and the typical size of the system (Janka et al. 2007). As long as the two computational problems mentioned above are concerned, it is customary to privilege numerical methods with a high order of accuracy (Leveque 2002). The use of multidimensional spectral methods (Gottlieb & Orszag 1977; Canuto et al. 1988, 2006) seems to be especially adequate.

Concerning the computational size difficulties, a rule of thumb (Gottlieb & Orszag 1977) claims in fact that for a given accuracy, spectral treatment requires five times less grid points per dimension than the ordinary second order finite difference algorithm. A computational factor of $5^6 = 15625$ could then be gained in modelling the transport equation. Consequently, solving the 6-D transport problem in a reasonable time while using a spectral algorithm and massive parallelisation seems possible. In this article, we shall describe the numerical methods that can be used in solving the sole transport equation for radiative particles and testing such an economy in computational time.

¹ The main difference between the two concepts is that in the transport equation, the collision term only describes interactions between neutrinos/photons and external medium (atoms, nuclei or electrons). (Herein after, we shall refer to neutrinos and photons as “radiative particles”, only using the term photon or neutrino when it turns out to be necessary). In the Boltzmann case, the collision terms also describe in principle interactions between the radiating particles; these are not relevant in our context. Therefore, we will try to avoid the term “Boltzmann equation” from now on.

From a mathematical point of view and adopting suitable approximations, the neutrino and photon transport equations are analogous in a wide range of settings. The abundant results on the photon transport equation will be however mainly used here for testing numerically our scheme².

In this work, the following assumptions are made:

1) As mentioned above, we assume the mass of the radiative particles to be zero (which for astrophysical neutrinos is a fairly reasonable assumption).

2) Neutrino and photon polarisation states are not taken into account, and are averaged on.

3) The interacting plasma is assumed to be in local thermal equilibrium. This physical oversimplification will allow for a much simpler treatment, by enabling to introduce the full thermal equilibrium limit in the equations.

4) For the simplicity of discussion, possible general relativistic terms are not taken into account. We believe that this aspect, though physically important in some astrophysical computations, will in no way change the behaviour of the numerical scheme, or the mathematical properties of the studied equations.

Using (6+1) general spherical coordinates in phase space, we will perform a numerical resolution using spectral methods based on Fourier/Chebyshev expansions, depending on the type of coordinates involved. This expansions will be performed in the physical space (classical spherical coordinates (r, θ, ϕ)) as well as in the momentum space (energy dependence and angular coordinates for the momentum part). Those methods have been developed and extensively used by our group and were described for the first time in Bonazzola & Marck (1990) (see also the review of Grandclement & Novak (2009)). Due to possible discontinuities arising on the space variable r , we will also propose a hybrid version of the code in which we use finite differences only in this dimension. A tentative conservative full spectral version including also a Chebyshev decomposition in r will be designed and tested as well. We shall show in different contexts relevant results in 5 dimensions at most, and give the corresponding CPU time obtained for every simulation, on single-processor runs of an ordinary computer with a clock frequency of 2.5 Ghz.

The paper is organised as follows: in Sect. 2, we present the general mathematical framework of the transport equation, alongside with typical physically motivated source terms for the equation. In Sect. 3 we present two asymptotic settings for physical transport of neutrinos and photons, namely the coherent transport case and the Fokker-Planck approximation. Those two limiting cases will be used as test problems in the ensuing numerical investigations. Sect. 4 will present the derivation of the transport equation in our chosen coordinates, as well as the possible mathematical problems that arise with this description; a few solutions will then be proposed to handle resolution in the most efficient way. Sect. 5 presents first numerical tests of the designed code, including time evolution for uniform distribution and full coherent transport using hybrid discretization. In Sect. 6 we show an application of the method to the transport of neutrino in a rotating neutron star by using an diffusion approximation in the inner part of the star and the exact solution in the outer region where the the diffusive approximation fails.

Appendix A presents an example of an explicitly particle-conservative form of the solved equations. Appendix B presents a solution to the full spectral approach in spherical symmetry,

² The only difference between general transport equation for neutrinos and photons, apart from a difference in cross section expressions, is the sign in front of the non-linear terms accounting for induced processes.

with an emphasis on the issue of conservation of the number of particles. **In Appendix C we show how the diffusion equation and telegraph equation are obtained. In our opinion, the telegraph equation is more suitable to treat neutrino transport when the matter velocity is close to the light velocity (super-novae problems). In fact the solution of the telegraph equation are such that the propagation velocity of the neutrino is always $\leq c/\sqrt{3}$. We want to point out that the telegraph equation can be numerically implemented with minor modifications with respect to the diffusion equation.**

2. Transport equation in 6 dimensions

2.1. Context and definitions

Let $f(x, y, z, p_x, p_y, p_z, t)$ be the distribution function in the phase space for a collection of particles, expressed in Cartesian-like coordinates. The transport equation will quantify the evolution of this distribution function with respect to collision terms, that describe the interaction of the radiative particle with other particle species of a plasma. The change in number of particles in the elementary phase space volume $D^3\mathbf{x} D^3\mathbf{p} = dx dy dz dp_x dp_y dp_z$ is then described by

$$\frac{D}{dt} f D^3\mathbf{x} D^3\mathbf{p} = CT, \quad (1)$$

where D/dt represents the total derivative and CT includes the collision terms. A reasonable assumption for neutrinos or photons is that between collisions with plasma particles (described in the collision terms), radiating photons/neutrinos travel in straight lines with no change in energy. This amounts to the absence of global forces acting on the radiating particles. In this context, the non-general relativistic transport equation in Cartesian coordinates takes the form:

$$\frac{1}{c} \frac{\partial f}{\partial t} + \omega^i \frac{\partial f}{\partial x^i} = CT, \quad (2)$$

where

$$\omega^i = \frac{p^i}{\|p\|}, \quad \omega \cdot \omega = 1, \quad (3)$$

c is the light velocity, and CT is a collision term that depends also on f .

2.2. The collision terms

Three different types of processes are expressed in collision terms:

- The rate of spontaneous emission of radiating particles by a particular process in the plasma will be expressed as $S(\nu, \mathbf{x})$; here \mathbf{x} models the spatial position, and ν is the radiative particle frequency (or its reduced energy E/h , where h is the Planck constant). A general assumption is that the emission is isotropic (i.e. matter itself does not have a preferred direction). This of course is only valid if our frame of reference is moving with the plasma.
- Absorption processes are expressed by a cross section $\sigma_a(\nu, \mathbf{x})$ and are also assumed to be isotropic.
- Scattering processes at a spatial position \mathbf{x} , from a radiating particle scattered from coordinates (ω, ν) within $(d\omega, d\nu)$ to (ω', ν') within $(d\omega', d\nu')$ is expressed by the cross section $\sigma_s(\mathbf{x}, \omega \cdot \omega', \nu \rightarrow \nu')$. Again, in agreement with the previous

assumption of isotropy for matter processes, this differential cross section only depends on the angle between the incoming and scattered radiating particle momentum, *via* the simple scalar product $\omega \cdot \omega'$.

We further assume for simplicity that radiative particles interact with only one species of the plasma, of particle mass m_0 . Using this energy scale we define an auxiliary distribution function

$$F = \left(\frac{h\nu}{m_0 c^2} \right)^2 f = \gamma^2 f, \quad (4)$$

where the notation γ is coined as the dimensionless energy for the radiative particle. This redefinition of the distribution function allows for a slightly simpler notation for the interaction terms, while the left hand side operator of Eq. 2 keeps the same form as applied to F . Once all those quantities characterising the interactions with matter are known, the collision term is determined by the formula:

$$\begin{aligned} CT = & n(\mathbf{r}, t) \{ S(\nu) - \sigma_a(\nu) F \\ & + \int_0^\infty d\nu' \int_{4\pi} d\omega' \sigma_d(\nu' \rightarrow \nu, \omega \cdot \omega') F(\nu', \omega') [1 \pm \frac{c^3}{2\nu^2} F(\nu, \omega)] \\ & - \int_0^\infty d\nu' \int_{4\pi} d\omega' \sigma_d(\nu \rightarrow \nu', \omega \cdot \omega') F(\nu, \omega) [1 \pm \frac{c^3}{2\nu'^2} F(\nu', \omega')] \} \end{aligned} \quad (5)$$

where $n(\mathbf{r}, t)$ is the interacting plasma density. For clarity, no spatial dependence of the chemical composition for the plasma is assumed; we finally write here interaction terms that are only proportional to the plasma density n . In the right hand side part, and besides the absorption and emission terms, the first integral term models the in-scattered neutrinos to coordinates to (ω, ν) within $(d\omega, d\nu)$. The second integral term models the out-scattered neutrinos, from (ω, ν) to (ω', ν') . σ_d is the differential scattering kernel for interactions. We have also included in front of the scattering integrals the quantum corrections due to induced processes for both types of radiating particles³. Only one term for each type of process is represented in an attempt for concision.

3. Different approximations

3.1. The coherent scattering

Consider the very low energy regime for the plasma and the radiating particles; the following assumptions are then made:

1) The plasma is at rest in our frame.

2) The ratio between the scattered particle energy $h\nu$ and the scattering target rest mass $m_0 c^2$ (be it a lepton or a hadron) is very small: ($\gamma = h\nu/m_0 c^2 \ll 1$). The velocity of scattering plasma particles will then always be neglected in this case.

Under the above assumptions, we crudely approximate that no energy exchange occurs, meaning that the energy of the scattered particle is the same as the incoming one. Therefore the scattering kernels writes:

$$\sigma_d(\nu \rightarrow \nu', \omega \cdot \omega') = \sigma_d(\omega \cdot \omega') \delta(\nu - \nu'), \quad (6)$$

where δ is the Dirac function. Here we give general expressions for the differential and total cross sections σ_d and σ_t , for photon

³ The plus sign holds for bosons (photons), the minus sign holds for fermions (neutrinos)

and neutrino scattering to electrons and hadrons. The total cross section is defined by:

$$\sigma_t = \int_0^\infty d\nu' \int_{4\pi} d\omega' \sigma_d(\nu \rightarrow \nu', \omega \cdot \omega'). \quad (7)$$

In the photon/electron case, the coherent scattering approximation leads to the well-known Thomson scattering cross sections:

$$\sigma_d^{Th} = 2r_e^2 (1 + (\omega \cdot \omega')^2) \delta(\nu - \nu'), \quad \sigma_t^{Th} = \frac{8\pi}{3} r_e^2 \quad (8)$$

where $r_e = e^2/(m_e c^2)$ is the classical radius of the electron, m_e being its mass.

In the neutrino/hadron interaction case, the differential cross section is usually reduced to the two leading orders in the angular decomposition, in the form:

$$\sigma_d^n = \frac{1}{4\pi} (A + B(\omega \cdot \omega')) \delta(\nu - \nu'), \quad \sigma_t^n = A \quad (9)$$

where A and B are constants depending on weak interaction parameters.

3.2. The Fokker Planck approximation

For a plasma particle, we denote by $\alpha = kT/m_0 c^2$ the thermal energy to mass energy ratio. In this section we assume that $\gamma \ll 1$ as before, $\alpha \ll 1$ and that the plasma, at rest in the laboratory frame, is in local thermodynamic equilibrium. In this context, we would like to describe low order energy redistribution in scattering processes. This is the setting of the Fokker-Planck approximation⁴. We obtain then for the photon distribution function $F = \gamma^2 f$ (Pomraning (1973) Eq.(8.62)):

$$\begin{aligned} \frac{\partial F(\gamma, \omega)}{\partial t} + \omega \cdot \nabla F(\gamma, \omega) = & n(\mathbf{x}, t) \sigma_{Th} \{-F(\gamma, \omega) \\ & + \frac{3}{16\pi} \int_{4\pi} d\omega' [1 + (\omega \cdot \omega')^2] F(\gamma, \omega') \\ & + \frac{1}{4\pi} \frac{\partial}{\partial \gamma} \left(\alpha \gamma^2 \frac{\partial}{\partial \gamma} + \gamma^2 - 2\alpha \gamma \right) \int_{4\pi} d\omega' F(\gamma, \omega') \\ & - \frac{3}{128\pi^2} \int_{4\pi} d\omega' \int_{4\pi} d\omega'' [1 - \omega' \cdot \omega'' + (\omega' \cdot \omega'')^2 - (\omega' \cdot \omega'')^3] \\ & \partial_\gamma (F(\gamma, \omega') F(\gamma, \omega'')) \} \end{aligned} \quad (10)$$

where we used here a number distribution function, as opposed to the energy distribution function I in Pomraning (1973). The equation is written in the reduced length unit of $\lambda_c = h/m_0 c$, $\lambda_c = 2.42 \cdot 10^{-10}$ cm being the Compton wavelength. As before, some variables dependencies in the distribution function are implicit. Absorption and emission terms are also not written here.

By using the Fokker Planck approximation, one can then replace the integral operator on the energy in the Eq.(10) by a differential operator, much easier to handle numerically. As mentioned in the introduction, the Fokker-Planck limit for transport will be considered as a test case in numerical investigations, alongside with the coherent scattering limit.

⁴ This approximation holds for photon nucleon collisions at plasma temperatures $< 10^{11}$ K and for temperature $T \leq 10^9 K^0$ and photon energy $h\nu \leq 0.1$ MeV. It is especially relevant in the context of X-ray astrophysics

From the Fokker-Planck equation we can define two typical times: the “isotropisation time” $\tau_{is} = 1/(n \sigma_{Th} c)$ describes the typical evolution of the angular distribution in phase space, whereas the “bosonisation time” $\tau_{Bo} = 1/(\alpha n \sigma_{Th} c)$ will be related to dynamical changes in the energy spectrum of radiative particles. Since $\alpha \ll 1$, $\tau_{Bo} \gg \tau_{is}$ holds; consequently, during the evolution, F will undergo an “isotropisation” process in a shorter timescale than the energy spectrum of the distribution function F will change significantly. If F is homogeneous and depends only on t and γ , then Eq.(10) reduces after integration on ω' and ω to the Kompaneet equation (Kompaneet 1957):

$$\frac{1}{c} \frac{\partial F}{\partial t} + n \sigma_{Th} \frac{\partial}{\partial \gamma} \left[\alpha \gamma^2 \frac{\partial F}{\partial \gamma} + (\gamma^2 - 2\alpha\gamma)F + \frac{1}{2}F^2 \right] = 0. \quad (11)$$

If we integrate both sides of the Eq.(11) on the dimensionless energy γ , we obtain, as expected, an equation which expresses the conservation of the number of photons:

$$\frac{\partial}{\partial t} \int_0^\infty F(\gamma, t) d\gamma = 0. \quad (12)$$

The steady state solution of Eq.(11) is a Bose distribution:

$$F(\gamma) = \gamma^2 f(\gamma) = 2\gamma^2 \left(\exp\left(\frac{\gamma - \mu}{\alpha}\right) - 1 \right)^{-1}, \quad (13)$$

The factor of 2 in the right hand side being related to photon polarisation. μ is an integration constant which physically represents the chemical potential.

The steady state solution is then a Bose distribution and *not* the usual Planck distribution that describes full thermal equilibrium. This is due to the fact that we have omitted the absorption and emission terms, and consequently constrain the photon number conservation given by the Eq.(12). This also justifies the term of “bosonisation” introduced above.

4. The transport equation in spherical coordinates

4.1. Definitions and properties

Starting from the quite general expression for the above equations, we specify now the geometry of our setting, as well as the attached chosen system of coordinates. Having in mind transport modelling in astrophysical (stellar) settings, the most natural geometry for this type of study is the spherical one. We here choose a set of 6-D spherical coordinates related to previously defined phase space vectors (r, ω) , and described by the variables $r, \theta, \varphi, \gamma, \Theta, \Phi$ as in Fig. 1.

The first three variables are the classical 3D spherical coordinates in physical space; Θ and Φ represent the angular dependence in the momentum space, whereas γ is a dimensionless measure of the photon (resp. neutrino) energy. In this system of coordinates, we can, from the expression in 6-D Cartesian-like coordinates, write the Liouville operator $\omega \cdot \nabla = \mathcal{L}$ using Jacobi matrix products for coordinate changes; one has however to keep in mind that in the new coordinate set, the angular variables in the momentum space are defined with respect to physical space angular coordinates; this of course slightly complicates the calculation. In the end, the operator \mathcal{L}_{sph} (in doubly spherical coordinates) reads (Pomraning (1973), and references therein):

$$\mathcal{L}_{sph} = \cos \Theta \frac{\partial}{\partial r} + \frac{1}{r} \left[\sin \Theta \cos \Phi \frac{\partial}{\partial \theta} + \frac{\sin \Theta \sin \Phi}{\sin \theta} \frac{\partial}{\partial \phi} - \sin \Theta \frac{\partial}{\partial \Theta} - \sin \Theta \sin \Phi \frac{\cos \theta}{\sin \theta} \frac{\partial}{\partial \Phi} \right], \quad (14)$$

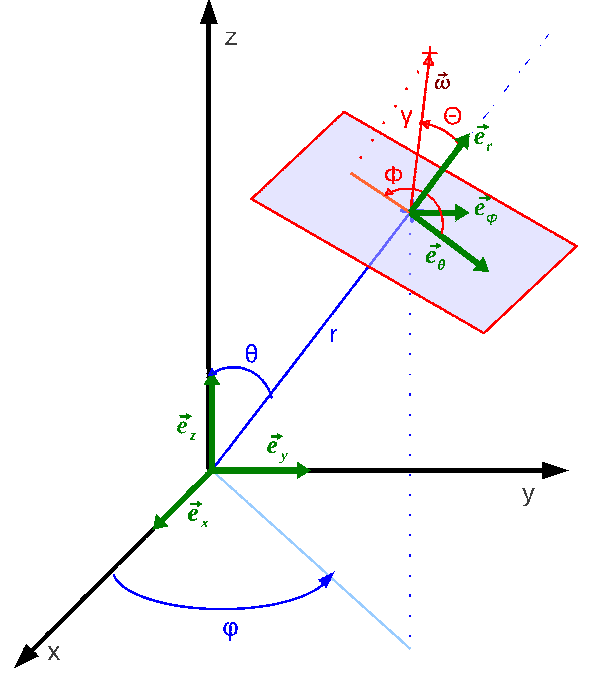


Fig. 1. Schematic representation of the 6d spherical coordinate in phase space. Note that a freedom exist for choosing the angular variable Φ up to a constant.

so that the general transport equation becomes

$$\frac{1}{c} \frac{\partial F}{\partial t} + \mathcal{L}_{sph} F = CT. \quad (15)$$

Let us note that it is also possible (and useful) to write this equation in a conservative form: see the Appendix A for a derivation of it.

In order to express integrals in source terms, the expression of the vector ω in the new system of coordinates is now required. We provide the Cartesian components $\omega_x, \omega_y, \omega_z$ of the vector ω as function of θ, ϕ, Θ and Φ :

$$\omega_x = \cos \Theta \sin \theta \cos \phi + \sin \Theta \cos \Phi \cos \theta \cos \phi - \sin \Theta \sin \Phi \sin \phi \quad (16)$$

$$\omega_y = \cos \Theta \sin \theta \sin \phi + \sin \Theta \cos \Phi \cos \theta \sin \phi + \sin \Theta \sin \Phi \cos \phi \quad (17)$$

$$\omega_z = \cos \Theta \cos \theta - \sin \Theta \cos \Phi \sin \theta. \quad (18)$$

The following properties hold ⁵:

$$\omega_x^2 + \omega_y^2 + \omega_z^2 = 1 \quad (19)$$

$$\mathcal{L}_{sph} \omega_x = 0, \quad \mathcal{L}_{sph} \omega_y = 0, \quad \mathcal{L}_{sph} \omega_z = 0. \quad (20)$$

Therefore, if the distribution function F depends only on ω , we have

$$\mathcal{L}_{sph} F(\omega_x, \omega_y, \omega_z) = 0. \quad (21)$$

⁵ In the Cartesian framework, the identities given by Eq.(20) are quite trivial: consider the Liouville operator \mathcal{L}_{cart} in Cartesian coordinate and Cartesian components:

$$\mathcal{L}_{cart} = v^i \frac{\partial F}{\partial x_i}$$

For $F = p_x, F = p_y$ or $F = p_z$ the above identities are fulfilled. This obviously holds then for any generic system of coordinates. Numerically, the relations in Eq.(20), or Eq.(21) can be used to assess the numerical accuracy of our resolution.

We shall finish this section by noticing that some terms of the Liouville operator \mathcal{L}_{sph} given by the Eq.(14) are singular for $r = 0$ and $\theta = 0, \pi$. Since the operator is itself regular, these terms correspond to coordinate singularities that shall cancel each other in the computation. We shall give an example of such cancellations in our case. Consider a spherical shell in physical space, for which $R_1 \leq r \leq R_2$ and $R_1 > 0$. Only singularity issues in $\theta = 0, \pi$ are then to consider. We first write a polynomial decomposition of the distribution in Cartesian-like coordinates:

$$F(x, y, z, \omega_x, \omega_y, \omega_z, t) = \sum_{i,j,k,A,B,C} C(t)_{ijkABC} x^i y^j z^k \omega_x^A \omega_y^B \omega_z^C. \quad (22)$$

In 6-D spherical coordinates, the singular terms in the Liouville operator given by the Eq.(14) are

$$\frac{\sin \Theta}{\sin \theta} \cos \Phi \left(\frac{\partial}{\partial \phi} - \cos \theta \frac{\partial}{\partial \Phi} \right). \quad (23)$$

In the above polynomial decomposition, we encounter two cases:

- For terms associated with coefficients of type $C(t)_{ijk00}$ (no dependence on ω), a spherical decomposition in (r, θ, ϕ) will lead to ϕ -dependent terms being factored by $\sin(\theta)$.

- For terms containing powers of $\omega_x, \omega_y, \omega_z$, their expression in Eqs.(16,17,18) ensures us that compensation will occur when the operator in Eq.(23) is applied.

The spectral representation of the considered fields is able to handle directly the specifics of the decomposition (see Bonazzola & Marck (1990); Grandclement & Novak (2009) for similar examples).

4.2. A simplified 2-dimensional case: The $\Theta = \pi/2$ discontinuity problem

We illustrate the prominent difficulties encountered in the analysis of this equation with a problem restricted to a spherically symmetric shell ($R_1 \leq r \leq R_2$) and with only coherent scattering allowed. The solution F for the distribution function will then only depend on the three variables t, r, Θ . We focus here on analyticity issues and the problem of boundary conditions. Under the above hypotheses, the transport equation simplifies to:

$$\begin{aligned} & \frac{1}{c} \frac{\partial F}{\partial t} + \cos \Theta \frac{\partial F}{\partial r} - \frac{\sin \Theta}{r} \frac{\partial F}{\partial \Theta} + n_e(r) (\sigma_{tot} F(t, r, \Theta) \\ & - \int_0^\pi \hat{\sigma}_{dif}(\cos \Theta \cos \Theta') F(t, r, \Theta') \sin \Theta' d\Theta') = 0, \end{aligned} \quad (24)$$

where $n_e(r)$ is a plasma density, σ_{tot} and σ_{dif} are respectively the total and differential cross section, and integration on the momentum angle Φ has already been performed. In order to perform a very simple analysis, we now artificially split the differential operator acting on F , so that we retrieve two advection equations. The radial advection part reads:

$$\frac{1}{c} \frac{\partial F}{\partial t} + \cos \Theta \frac{\partial F}{\partial r} = 0. \quad (25)$$

This is a first order equation, associated to an evolution with velocity $V = c \cos \Theta$. It propagates from the inner region of the shell to the outer one if $0 \leq \Theta < \pi/2$ ($\cos \theta > 0$). On the contrary, it propagates from the outer region to the inner one if $\cos \Theta < 0$. Consequently, in our geometrical setting, an inner boundary condition at $r = R_1$ has to be imposed for $\Theta \leq \frac{\pi}{2}$ (incoming flux) and an outer condition at $r = R_2$ for $\Theta > \pi/2$ (re-entering flux).

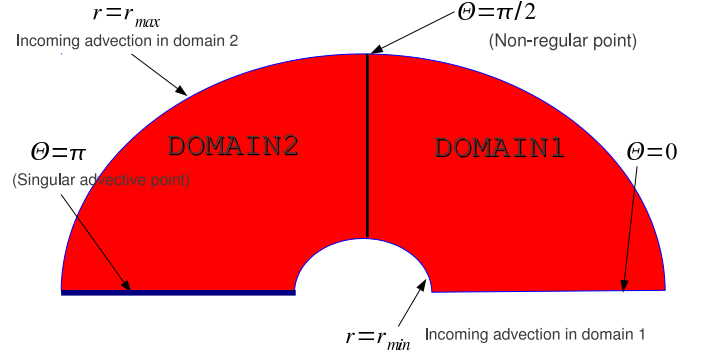


Fig. 2. 2d representation of the computational domain.

If we now consider the second advection term

$$\frac{1}{c} \frac{\partial F}{\partial t} - \frac{\sin \Theta}{r} \frac{\partial F}{\partial \Theta} = 0, \quad (26)$$

the analysis is here simpler: propagation occurs always from $\Theta = \pi$ to $\Theta = 0$ in the computational domain. However, the vanishing of $\sin \Theta$ at $\Theta = \pi$ shows a degenerate behaviour at this point: no advection in Θ occurs, therefore no boundary treatment is needed.

Coming back to the full Eq.(24), it is now expected that regularity issues in the numerical solution will arise⁶ across the surface $\Theta = \frac{\pi}{2}$, due to different radial advective directions on both sides. For example, a boundary condition value for F can be freely set to

$$F(t, R_1, \Theta \leq \frac{\pi}{2}) = A, A \in \mathbb{R}, \quad (27)$$

whereas the values $F(t, R_1, \Theta \geq \frac{\pi}{2})$ are advected from the computational domain and therefore uncontrolled. To overcome the numerical problems associated with this behaviour, we split our computational domain (here, a spherical shell) into two angular domains $D_1(r \in [R_1, R_2], \Theta \in [0, \frac{\pi}{2}])$ and $D_2(r \in [R_1, R_2], \Theta \in [\frac{\pi}{2}, \pi])$ (see Fig. 2). To ensure particle number conservation across the two domains, we must enforce continuity of the flux on $\Theta = \frac{\pi}{2}$. This provides us with an incoming boundary condition in Θ to impose for the solution F in D_1 .

5. Numerical tests

5.1. Overview of the computational setting and approach

We present below specific tests related to the spectral resolution of the (homogeneous or not) transport equation. As outlined above, our computational grid covers a physical shell $R_1 \leq r \leq R_2$ (see section 6 for the treatment of the singularity at the center) split into two domains $D_1[0 \leq \Theta \leq \frac{\pi}{2}]$ and $D_2[\frac{\pi}{2} \leq \Theta \leq \pi]$. A typical value for our domain size is $\frac{R_2}{R_1} = 5$. Unless otherwise stated, spectral decompositions are

⁶ We describe a function F as regular if it is of class C^p with p large enough to have a fast convergence in the spectral expansion.

performed using a Chebychev representation on the r, Θ and γ direction, whereas a Fourier decomposition is performed for the remaining angular dependencies. The spectral decomposition of a scalar field is then very much similar to the one described in (Bonazzola et al. 1999), however performed in six dimensions instead of the usual three. For general information on numerical use of spectral methods as intended here, we direct the reader to the recent review of (Grandclement & Novak 2009).

If we denote by T_i the i^{th} order polynomial in the classical Chebyshev basis and by $Y_{\ell m}(\theta, \varphi)$ the 3D spherical harmonics component of order (ℓ, m) , a decomposition of the 6D time-dependent distribution function is given by:

$$F(r, \theta, \varphi, \gamma, \Theta, \Phi, t) = \sum_{i, \ell, m, A, B, C} C_{i\ell m ABC}(t) T_i(r) Y_{\ell m}(\theta, \varphi) T_A(\gamma) T_B(\cos(\Theta)) \cos(C\Phi), \text{Ceven},$$

$\sin(C\Phi), \text{Codd}$.

where we manipulate the set of coefficients $C_{i\ell m ABC}(t)$ as the representation of $f(r, \theta, \phi, v, \Theta, \Phi, t)$ at any time. The representation above assumes a symmetry with respect to the (ω_y, ω_z) plane to obtain this particular dependence in Φ . Otherwise, all terms of the Fourier decomposition have to be considered. All numerical operations are then performed in the coefficient space, and using the product base described in the above expansion. Imposition of boundaries is performed using a Tau approach (Gottlieb & Orszag 1977). In particular, differential functions composing the Liouville operator are expressed as matrices acting on the coefficient vectors $C_{i\ell m ABC}$. A semi-implicit resolution in the Appendix B also uses Tau like methods for operator inversion, handling numerically vectors of spectral coefficients $C_{i\ell m ABC}$.

In this section, the chosen explicit time marching scheme is a classical second order Adams-Bashforth one, minimizing dissipation. Again, only spectral coefficients are updated.

The chosen computational domain is the shell set of domains described in the previous section ; Tau-matching is performed at the innermost and outermost sphere, as well as at the $\Theta = \pi/2$ interface. In the diffusion transport problem of section 6, a central sphere-like domain is added to the setting, in which the representation of functions is the same as in the rest, and for which numerical solutions have of course to be matched through the outer interface (see again Section 6).

5.2. Time evolution of a uniform distribution

We assume our domain to be filled by a uniform plasma of constant density $n = n_0$, which at first is interacting with our radiating particles only through coherent scattering. Absorption and emission are disabled (which ensures particle number conservation during the computation) and we start with the artificial initial condition for the distribution function:

$$F(\theta, \phi, \Theta, \Phi, t = 0) = \left(1 + 2\omega_x + \omega_y + \frac{1}{2}\omega_z\right)^4, \quad 0 \leq \Theta \leq \frac{\pi}{2}$$

$$F(\theta, \phi, \Theta, \Phi, t = 0) = 0, \quad \frac{\pi}{2} \leq \Theta \leq \pi. \quad (28)$$

Taking advantage of the properties of the Liouville operator described in Eq. (20), we know that at any time of the computation, $\mathcal{L}_{sph} F = 0$. Monitoring the numerical validity of this property is another way to assess accuracy of our approach.

Fig 3 presents particle conservation for this setting over time. The slow drift we encounter only occurs at the level of com-

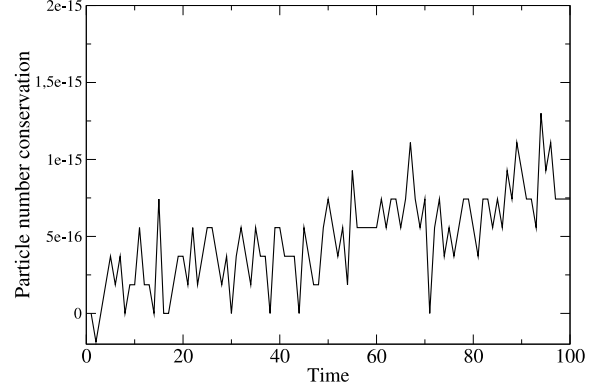


Fig. 3. Relative particle number conservation for the coherent time evolution of a uniform distribution

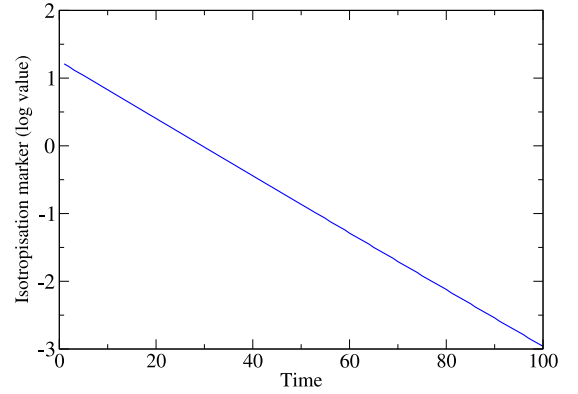


Fig. 4. L^0 norm of the non-isotropic terms in the spectral decomposition of the distribution function: this is computed as the ratio between the coefficient of the constant (isotropic) term in the decomposition, rescaled to the sum of all other coefficients. This serves as a reliable marker for the isotropisation process in the evolution.

puter roundoff. We consistently obtain a relative error in particle number count smaller than 5.10^{-15} in double precision, on timescales much larger than the dynamical timescale of the simulation. The isotropisation process of the distribution function due to coherent scattering is also displayed on Fig 4. For those results, the number of points used is $(N_r, N_\theta, N_\phi, N_\Theta, N_\Phi) = (33, 17, 16, 25, 16)$. A resolution time step takes about 20 seconds in CPU time.

Using the same initial spatial profile for the distribution, we now allow for energy dependence and non-coherent scattering by implementing the energy-dependent source terms set in Eq. (10). The initial energy distribution is set to be a black body one, at a temperature half the one of the plasma ($kT/m_e c^2 = .01$ in our units). Conservation of the number of photons ensures that F will approach a Bose distribution (see Eq. (13)) over time. Using $N_\gamma = 33$ points in the energy dimension, a computational time step takes about 33s.

In Fig. 5 we can observe the transition made from the initial energy distribution to the final one, and appreciate the possible observation of a low-energy condensation that is accessible even

with a very limited number of points. It is obvious that a specific treatment of the low energy regime (by allocating a specific spectral decomposition domain to this region, and increasing the degree of spectral decomposition) would be necessary to study such an effect quantitatively ; however, the goal of this work is only to convince oneself that such study is, indeed, possible with limited computational resources.

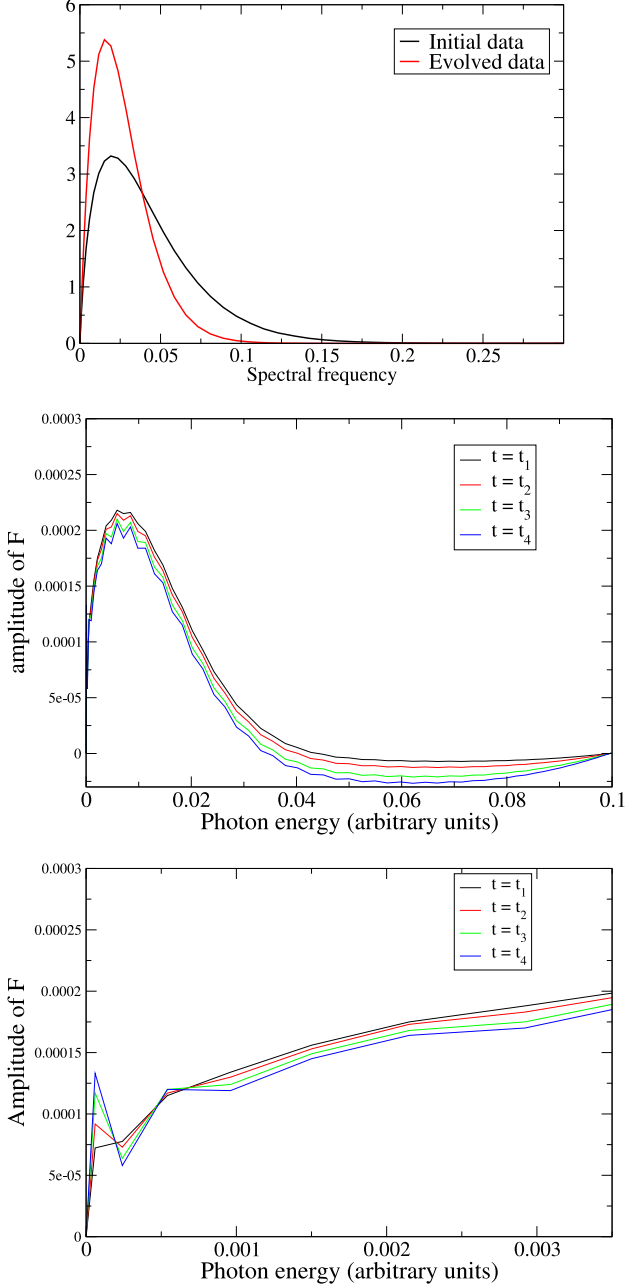


Fig. 5. Evolution of the energy distribution of F , showing the transition to a Bose distribution and a low-energy condensation. The middle and lower panel display this energy distribution at four arbitrary consecutive times. No smoothing of the data has been performed.

5.3. 5d coherent transport in a shell

We consider a spherical shell enclosing black body radiating particles through its outer surface $R = R_2$. In the computed shell domain resides a plasma with the following arbitrary density:

$$n(r, \theta, \phi) = n_0[1+0.1(r \sin \theta \cos \phi \cos \theta)][1 - (1 - r/R_1)/(1 - r/R_2)]^8. \quad (2)$$

This plasma triggers coherent scattering, but again emission and absorption processes are disabled for simplicity: we only want to monitor the behaviour of a transport process. The shell is initially free of any radiating particles, and the central object emits continuously a particle flux following a Lambert law; this leads to the inner boundary condition for F :

$$F(R_1, \theta, \phi, \Theta, \Phi) = F_0 \cos \Theta. \quad (30)$$

This problem will be treated spectrally, except for the radial direction r where we use a simple first order finite-difference scheme. The reason behind it is a better treatment of the discontinuity and a reduction of the overshooting in this direction that inevitably appears. Grid point numbers are $(N_r, N_\theta, N_\phi, N_\Theta, N_\Phi) = (129, 17, 16, 25, 16)$, and a time step is around 216s wall clock time, again on a single core. Fig 6 presents distribution function profiles at different time steps in the case of an optically thin regime (optical depth with respect to the coherent scattering is set to zero), or an optically thick one (in our arbitrary units, the optical depth is set to 5). We are able to represent without any problem the beaming effect occurring during the 5d transport, which is also coupled to a large attenuation in the second case (the loss of luminosity by 5 orders of magnitudes on a short distance is not altering the code precision, as can also be seen by a check on the particle number conservation). It is obvious that in the transparent case, an excessive beaming will eventually lead to resolution issues in the angular directions ; this issue can be cured again (at least locally) by treating a low Θ region separately (domain decomposition for the spectral treatment) and assuming a better resolution at small angles. It is obvious that an open free streaming region cannot be handled by our approach in a clean way : one would have then to resort to less sophisticated descriptions of the particle flux, and match to the exact solver. We observe a clear discontinuity of F at the edge $r = R_1$ of the domain, assuming a non-zero optical depth; it is a consequence of our rather abrupt assertion for the radiation source to be a pure Lambertian object. A more sophisticated approach for the source would allow to get rid of such a feature, although this computation proves that the code behaves well even in ill-posed settings.

5.4. Stability and convergence conditions

We end this section by expliciting the stability conditions constraining the model evolution. In general, the maximal allowed value for the time increment Δt is determined by the most stringent Courant condition in each dimension. In the 5-D hybrid advection code above, the stability condition gives an order of the timestep limit as the minimum of the following values:

$$\Delta t_r = \frac{(R_2 - R_1)}{N_r^2}, \Delta t_\theta = \frac{1}{N_\theta}, \Delta t_\phi = \frac{1}{N_\phi}, \Delta t_\Theta = \frac{1}{N_\Theta^2}, \Delta t_\Phi = \frac{1}{N_\Phi}, \quad (31)$$

with notations introduced above. The most severe limitations are given in the r and the Θ dimensions. In the example showed in Fig.6, the timestep limit is $\Delta t = 5 \times 10^{-3}$ (2000 timesteps) for $N_r = 129, N_\Theta = 17$.

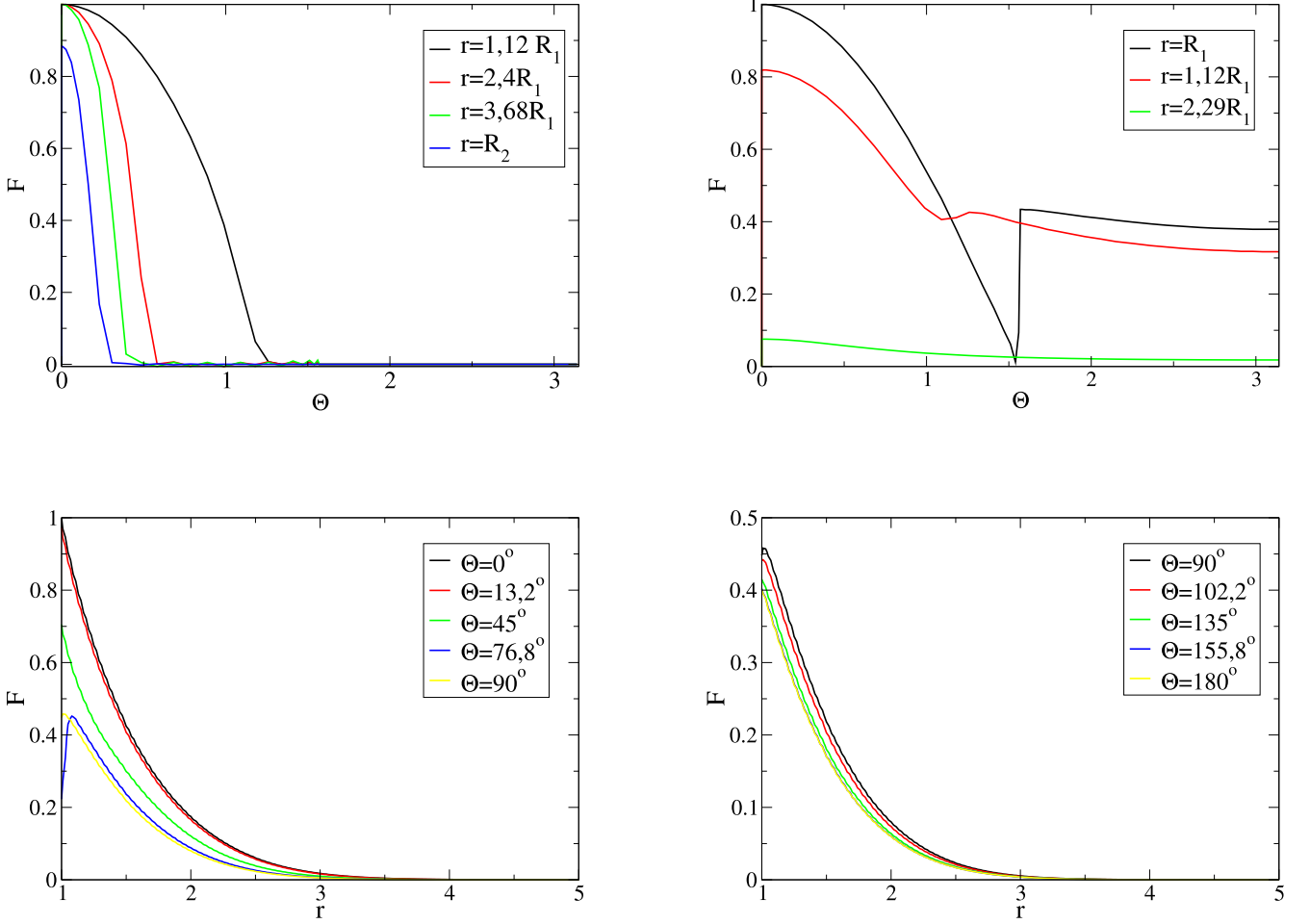


Fig. 6. Profiles of the distribution function F along the directions r and Θ at time $t = 4, 2$ in our units. The upper left panel represents angular profiles assuming zero optical depth for coherent scattering, whereas the upper right one corresponds to an optical depth of 5 in our units. The two lower panels are radial profiles at different angles for the same time, and for an optical depth of 5. The boundary values correspond to the thermal emission of a Lambertian object (a perfect black body here), and a non-re entrant condition for the outer radius.

6. An example: neutrino transfer in a rotating neutron star

The neutrino transfer in a hot rotating neutron star is a first step towards solving the problem of a cooling neutron star (NS). We consider a slowly rotating steady state neutron star with a given neutrino distribution and we apply all the machinery described above in computing the neutrino flux as function of time. We consider this academic example simple enough but containing difficulties that are present in a wide class of problems, like the evolution of a proto-neutron star (PNS) for which hydrodynamics and neutrino transfer are coupled. Once again, the emission and absorption coefficients are omitted because their presence does not add numerical difficulties, and their absence allows us to test performances of the code like neutrino conservation, continuity of the solution. In fact emission and absorption terms can hide defects of the solution.

In what follows, we consider a slowly rotating NS (The

surface of the NS is only weakly deformed by the rotation), on an axisymmetric equilibrium configuration determined by an arbitrary equation of state.

Because of the symmetry, the transfer problem reduces to a 5-D problem: the variables are r , θ , Θ , Φ , the energy of the neutrinos E plus the time t .

In the collision operator, only the nucleon scattering is taken into account, and the approximation of coherent scattering is used.

Because of the slow rotation, the plasma can be considered at rest. Note that this approximation also holds for a PNS cooling and shrinking gently. For a fast rotating neutron star, described in a next section, we shall give an hint on how to treat the problem.

As already said, this example is used to show different difficulties that are present in solving the above problem and how to overcome them. For simplicity and without any loss of generality we have chosen an analytic profile of mass density

$$n(r, \theta) = n_0 \left[1 - \left(\frac{r}{R_*} \right)^2 + \frac{1}{2} \left(\frac{2\pi r}{P c} \sin \theta \right)^2 \right]^{1/(\gamma-1)}, \quad (32)$$

where n_0 is the central density, R_* the radius of the star, c the light velocity, P the rotation period and γ mimics the polytropic index ($4/3 \leq \gamma \leq 2$). For $n_0 = 4 \times 10^{14} \text{ g.cm}^{-3}$, $R_* = 15 \text{ km}$, $\gamma = 5/3$ and $P \geq 3 \text{ ms}$, the mass of the star is $1.4 M_\odot$. The above analytic expression of the matter density has the advantage to be flexible and to mimic different equations of state. For realistic applications, the profile density must be computed by solving the G.R. equations for a steady state configuration. In this case, the value of the mass density $n(r, \theta)$ is given in the sampling points of the variables r and θ . The numerical grid defined in a such a way will be called the *master grid*.

The main difficulties addressed in our example are:

1. How to handle the singularity at the center.
2. How to treat the large range of opacities, especially the strong dependence on the neutrino energy E . Recall that the neutrino cross section behaves as $\sim E^2$

We have not yet solved the $r = 0$ singularity problem in the above formalism. Moreover, the opacity $\tau = n \sigma_t$ (σ_t being the total scattering cross section) close to the center of the star can be so large that it would require an excessively small time step.

In order to bypass this difficulty we propose to cut the r domain in two regions : a first one running from 0 to R_{in} ($0 \leq r \leq R_{in}$) and a second one running from R_{in} to R_* ($R_1 \leq r \leq R_{in}$). The value of $R_{in}(E)$ is determined in a such a way that for a given energy E the opacity τ in the domain $0 \leq r \leq R_{in}$ is larger than a critical value τ_c for which the diffusion approximation holds. Numerical experiments have shown that in the above example, τ must be

$$\tau_c \geq 2 \text{ km}^{-1}, \quad (33)$$

in order that the diffusion approximation holds and and

$$\tau \leq 10 \text{ km}^{-1}, \quad (34)$$

to have an acceptable time step to solve the exact transfer equation.

The way to proceed is the following : solve the diffusion equation (See App. C)

$$\frac{\partial F_0(r, \theta, E, t)}{\partial t} - \tau(r, \theta, E, t) \Delta F_0(r, \theta, E, t) - \nabla_j F_0(r, \theta, E, t) \nabla^j \tau(r, \theta) = S(r, \theta, E, t), \quad (35)$$

in the domain $0 \leq r \leq R_{in}$. Note that, as it was already said, the absorption and emission terms in S is put to 0 in the present example. Then solve the exact transfer equation in the domain $R_1 \leq R_*$ and then match the two solutions (Here $S(r, \theta, E, t)$ are the source terms generated by absorption and emission and Δ is the Laplacian in spherical coordinates.

$$\Delta = \frac{\partial^2}{\partial r^2} + \frac{2}{r} \frac{\partial}{\partial r} + \frac{1}{r^2} \left(\frac{\partial^2}{\partial \theta^2} + \frac{\cos \theta}{\sin \theta} \frac{\partial}{\partial \theta} \right). \quad (36)$$

The diffusion equation is solved with a semi-implicit scheme (Gottlieb & Orszag 1977). After expansion in Legendre polynomials $P_l^0(\theta)$ a second order time scheme can be written with obvious notations at the time t^{j+1} for a given energy E

$$F_{0l}^{j+1}(r, E) - \tau_{max} \Delta_l F_{0l}^{j+1} \frac{dt}{2} = F_{0l}^j - \frac{dt}{2} \tau_{max} \Delta_l F_{0l}^j + \left[(\tau(r, \theta E) - \tau_{max}) \Delta F_0 - \nabla_j F_0 \nabla^j \tau + S \right]_l^{j+1/2} dt, \quad (37)$$

where

$$\Delta_l = \frac{d^2}{dr^2} + \frac{2}{r} \frac{d}{dr} - \frac{1}{r^2} l(l+1), \quad (38)$$

with τ_{max} the maximum value of τ in the domain and dt the time step. The terms at time $j + 1/2$ are obtained by extrapolation using the terms at the time $j - 1$ and j . The singularity at $r = 0$ is handled by choosing an expansion on a polynomial basis that has good analytical properties at $r = 0$. The scheme is unconditionally stable (Bonazzola et al. (1999)). Moreover, in Eq.(37) the matrix of the operator at the L.H.S can be reduced to a penta-diagonal matrix.

6.1. The mono energetic case

In this section the conservative formulation of the transport equation will be used and the dependence of F on E will be omitted .

We take an averaged cross section σ^D

$$\sigma^D = \sigma_{\nu n}^D + \sigma_{\nu p}^D, \quad (39)$$

from Bruenn (1985) : for neutrino neutron scattering

$$\sigma_{\nu n}^D = A_{\nu n} \left(1 - \frac{1}{3} \omega \cdot \omega' \right), \quad \sigma_{\nu n}^T = 4 \pi A_{\nu n}, \quad (40)$$

and for protons

$$\sigma_{\nu p}^D = A_{\nu p} \left(1 - \frac{1}{10} \omega \cdot \omega' \right), \quad \sigma_{\nu p}^T = 4 \pi A_{\nu p}. \quad (41)$$

Let us consider some mono energetic neutrinos with $E = 3 \text{ MeV}$. We take $R_{in} = 11.4 \text{ km}$. We form two domains, $0 \leq r \leq R_{in}$ and $R_{in} \leq r \leq R_*$. In the first domain the optical depth is $\tau \geq 5$. In this domain we shall solve the diffusion equation by using spectral methods. The grid in the first domain has a Chebyshev decomposition for r sampling points (the θ sampling points are unchanged). In the second domain a uniform grid is defined. (We use the hybrid version of the transport equation, i.e. the r dependence of the variables are treated with a finite difference scheme). We consider a $1.41 M_\odot$ neutron star with a rotation frequency of 637 Hz (corresponding to $\Omega = 4000 \text{ rad.s}^{-1}$), and a ploytropic index $\gamma = 5/3$. The matter density is given by Eq.(32).

We define the matter density function $n(r, \theta)$ on the two grids⁷. We shall introduce the obvious notations $n_1(r, \theta)$, $n_2(r, \theta)$ and F_1, F_2 defining quantities in the domains (1) and (2).

6.2. Matching

Matching of the two solutions F_1 and F_2 at $r = R_{in}$ cannot be exact. In fact the solution F_1 obtained with the diffusion approximation contains only two moments F^0 and F^1

$$F_1(r, \theta, \Theta, \Phi, t) = F_1^0(r, \theta, t) + 3F_1^1(r, \theta, t) \cdot \omega, \quad (42)$$

⁷ In our case, the function $n(r, \theta)$ is analytic, but in a general case, one would have to perform an interpolation.

where (see App. C)

$$F_1^1 = -\frac{1}{3\tau} \nabla F_1^0. \quad (43)$$

On the contrary, the exact solution F_2 contains a large number of moments, consequently the matching cannot be exact.

To overcome this difficulty we perform an averaged matching that conserves the number of neutrinos and we impose an averaged continuity of F_1 and F_2 ⁸.

Before we explain the way to proceed, we have to recall that the solution of the second order diffusion equation admits two homogeneous solutions $H_1(r, \theta, t)$ and $H_2(r, \theta, t)$. One of the homogeneous solution is used to handle the coordinate singularity at $r = 0$ ⁹, the second one is used to satisfy the boundary conditions at $r = R_{in}$ for each value of θ and at each time t_j .

As it was already stated, boundary conditions at $r = R_{in}$ can be imposed on the solution of the full transport equation $F_2(r, \theta, \Theta, \Phi, t)$ only in the case $0 \leq \Theta < \pi/2$ (see section 2). At each time step t_j we impose the following boundary conditions (B.C.) for F_2

$$F_2(R_{in}, \theta, \Theta, \Phi, t_j) = F_2(R_{in}, \theta, \pi/2, \Phi, t_j) + \beta \cos \theta, \quad (44)$$

where β is determined together with the boundary conditions of F_1 , so that

$$\begin{aligned} & \int_0^{2\pi} d\Phi \int_0^\pi F_1(R_{in}, \Theta, \Phi) d\Theta \\ &= \int_0^{2\pi} d\Phi \left[\int_0^{\pi/2} (F_2(R_{in}, \theta, \Theta, \Phi) + \beta \cos \Theta) d\Theta \right. \\ & \left. + \int_{\pi/2}^\pi F_2(R_{in}, \theta, \Theta, \Phi) d\Theta \right], \end{aligned} \quad (45)$$

and the flux conservation

$$\begin{aligned} & \int_0^{2\pi} d\Phi \int_0^\pi F_1(R_{in}, \theta, \Theta, \Phi) \cos \Theta d\Theta = \\ & \int_0^{2\pi} d\Phi \left[\int_0^{\pi/2} (F_2(R_{in}, \theta, \Theta, \Phi) + \beta \cos \Theta) \cos \Theta d\Theta \right. \\ & \left. + \int_{\pi/2}^\pi F_2(R_{in}, \theta, \Theta, \Phi) \cos \Theta d\Theta \right]. \end{aligned} \quad (46)$$

By taking into account the Eqs.(43) and (42), the system of equations Eqs.(45) and (46) reads (matching the distribution function)

$$\begin{aligned} 4\pi F_1^0(R_{in}, \theta) &= \int_0^{\pi/2} F_2(R_{in}, \theta, \pi/2, \Phi) d\Phi \\ &+ \int_0^{2\pi} d\Phi \int_{\pi/2}^\pi F_2(R_{in}, \theta, \Theta, \Phi) d\Theta + \pi\beta, \end{aligned} \quad (47)$$

and as for the flux conservation

⁸ In the same spirit as the Marshak approximation for imposing boundary conditions.

⁹ For more details see Bonazzola et al. (1999).

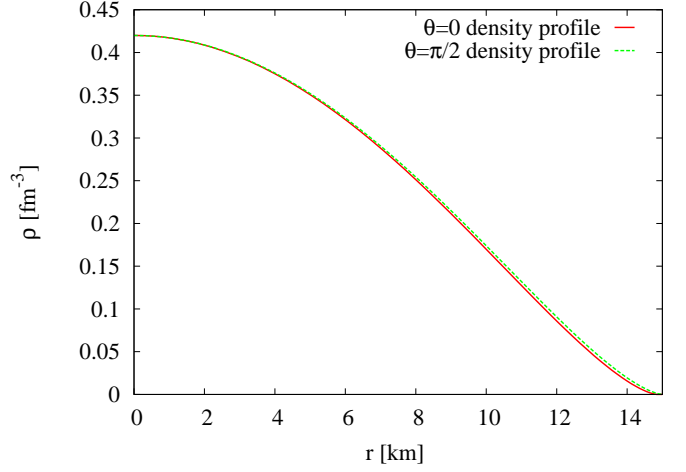


Fig. 7. Neutron star barionic density profile, equatorial and polar density.

$$\begin{aligned} -\frac{4\pi}{3\tau} \frac{\partial F_0(R_{in}, \theta)}{\partial r} &= \int_0^{2\pi} d\Phi [F_2(R_{in}, \theta, \pi/2, \Phi) \\ &+ \int_{\pi/2}^\pi F_2(R_{in}, \theta, \Theta, \Phi) d\Theta] + \frac{2}{3}\pi\beta. \end{aligned} \quad (48)$$

As it was already stated, the unknown of the system are the boundary condition $F_1((R_{in}, \theta, t_j))$ and the coefficient β . Note that once $F_1(R_{in}, \theta, t_j)$ is given, its derivative with respect to r is known.

6.3. The multi-energy case

To treat a full energy spectrum, we discretise the energy spectrum. Let N_E be the number of sampling points and E_j the neutrino energies. The straightforward way to proceed is to define two secondary grids for each value of the energy E_j . Actually we do not need so many secondary grids, we can form groups of energies for which the relations given by Eqs.(33) and (34) hold. In our example for a neutrino energy spectrum with $1.5 \text{ MeV} \leq E \leq 15 \text{ MeV}$ a partition of the spectrum can be, for instance, such as described in table 1, which shows that only 6 secondary grids are required.

Here we present the results: The matter density distribution at the pole and at the equator of a rotating star with a rotation frequency of 637 Hz is shown in Fig. 7. In what follows, we shall use this rotation frequency.

Figure 8 shows the initial neutrino distribution function at time $t = 0$. This distribution depends only on r . The code runs until the flux at the surface of the star reaches its maximum at the time $t = T$ (See Fig. 9).

Figures 10 show the neutrino distribution function for $\theta = 0$ and $\theta = \pi/2$ averaged on Θ and Φ at energies respectively of 1.6 MeV, 2 MeV and 5 MeV. The star on the $r = R_{in}$ axis indicates the separation of the two grids. The optical depth at $r = R_{in}$ was chosen to be $\sigma n = 5 \text{ km}^{-1}$. Note the good matching of the two solutions.

Figure 11 shows the neutrino distribution function averaged on θ and Φ at the grids separation point in the case of a neutrino energy $E = 2 \text{ MeV}$. Note that that the function is very smooth across the axis $\Theta = \pi/2$

Table 1. Spectrum partition for different radius.

Energy (MeV)	Radius R_{in} (km)
1, 5	4.35
2.0	7.7
3 – 4	11.0
5 – 7	13.3
8 – 10	13.8
11 – 15	14.35

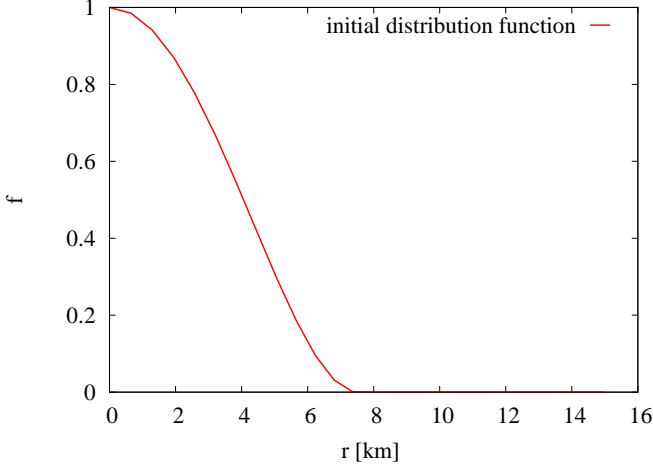
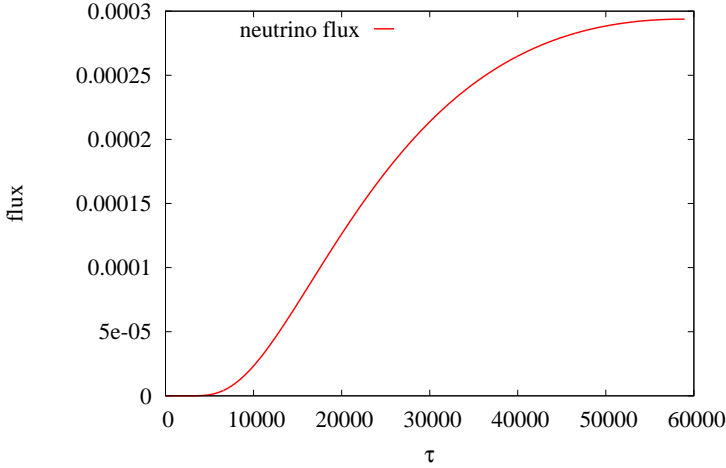

Fig. 8. Initial conditions: Neutrino distribution function at time $t = 0$. This initial distribution is the same for the three energies taken into account (1.6 MeV, 2 MeV, 5 MeV)

Fig. 9. Neutrino flux at the surface of the star, with a neutrino energy of 2 MeV. The x axis represents the time in free fly unit $\tau = R/c$

Figure 12 shows shows the neutrino distribution function $f(R, \theta, \Theta, \Phi, 2 \text{ MeV})$ averaged on θ and Φ at the surface of the star. Note that the boundary conditions (outgoing flux) is exactly fulfilled.

Fig. 13 shows the neutrino conservation relative error as a function of time (with a neutrino energy $E = 2 \text{ MeV}$).

The diffusion approximation holds only when the opacity $\sigma n \rightarrow \infty$. In order to estimate the relative error as function of the thickness σn , the error ϵ is defined by

$$\epsilon = \frac{1}{P_0} \left(\sum_{l=2}^6 P_l^2 \right)^{\frac{1}{2}}, \quad (49)$$

where

$$P_l = \int_0^{2\pi} d\Phi \int_0^\pi \sin \Theta d\Theta \int_0^\pi P_l^0(\Theta) F(R_{in}, \theta, \Theta, \Phi, T) \sin \theta d\theta, \quad (50)$$

where, again, T is the time at the end of the run and $P_l^0(\Theta)$ are the Legendre polynomials.

Fig. 14 shows the dependence of the error ϵ on the optical thickness σn . When moments $P_{>2} = 0$, the error vanishes to a good approximation.

Analogous errors are found for different energies. It seems that an optical thickness $n\sigma \sim 5 \text{ km}^{-1}$ at the grids separation is a good compromise.

6.4. Convergence

An efficient test to check the accuracy of the code consists in studying the behavior of the amplitude of Chebyshev-Fourier coefficients as a function of their order. Fig. 15 shows the behaviour of the Chebyshev normed coefficients of the expansion in θ of the averaged solution.

$$G_\theta(r, \theta) = \int_0^{2\pi} d\Phi \int_0^\pi F(r, \theta, \Theta, \Phi, T) \sin \Theta d\Theta. \quad (51)$$

For $r = R_{in}$ and $r = R$ we see that there exists a break of the slope of the coefficients when the amplitude of the coefficients is $\sim 10^{-8}$. This behavior is due the fact that the matter density derivative with respect to θ is discontinuous close to the surface of the star (See Fig 1).

Note that only 8 coefficients are required to reach an accuracy of 10^{-5} . Here the number of coefficients is 17, but the odd coefficients vanish because of the equatorial symmetry of the problem.

Fig. 16 shows the Chebyshev normed coefficients of the averaged functions $G_\theta(r)$

$$G_\theta(r, \Theta, T) = \int_0^{2\pi} d\Phi \int_0^\pi F(r, \theta, \Theta, \Phi, t) \sin \theta d\theta. \quad (52)$$

Analogously, Fig. 17 shows the behaviour of the Φ coefficients. Note that all the coefficients vanish, as expected, exponentially when their number increase.

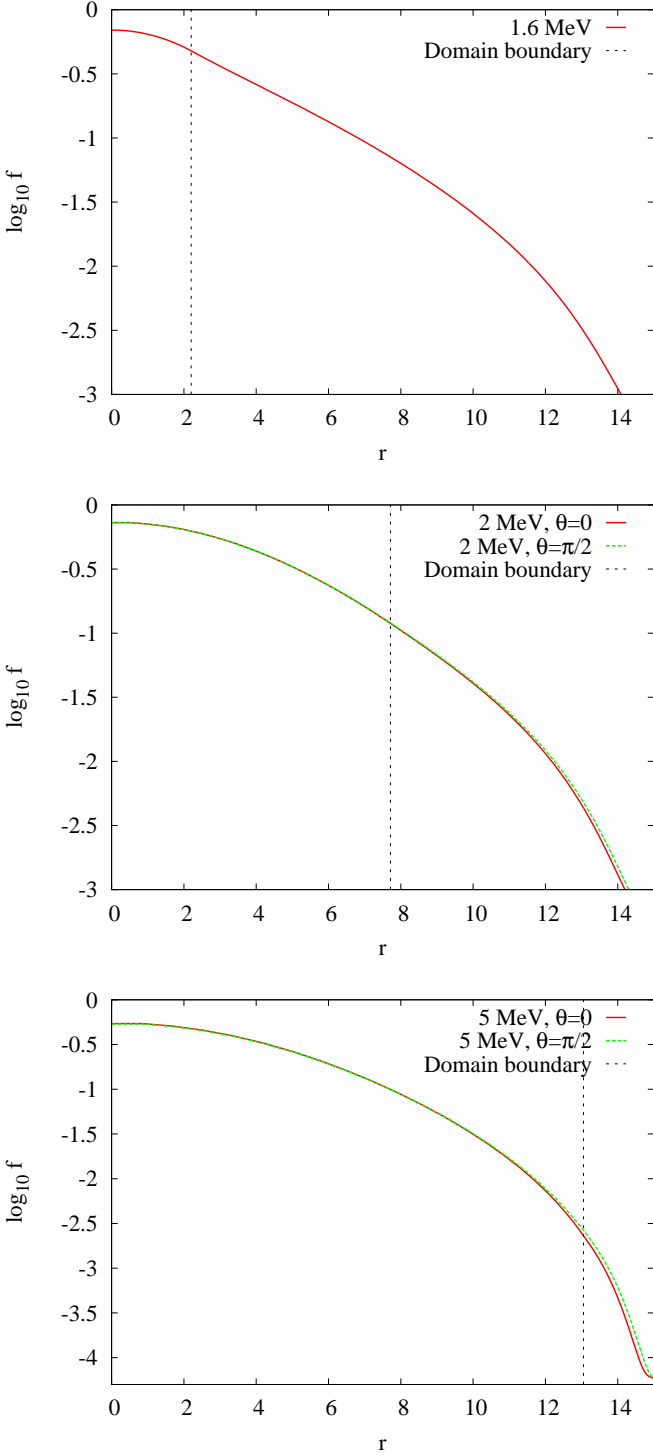


Fig. 10. 1.6 MeV, 2 MeV and 5 MeV neutrino distribution for $\theta = 0$ and $\theta = \pi/2$ at time $t = T$ (in the 1.6 MeV, only one is represented because both $\theta = 0$ and $\theta = \pi/2$ are indistinguishable). The separation on the x axis marks the boundary of the two grids (see text).

6.5. Fast rotating star

In the case of a fast rigidly rotating star, the centrifugal force strongly deforms the surface of the star. The deformation generates a derivative discontinuity of the matter density in the spherical grid, where the steady state configuration of the star

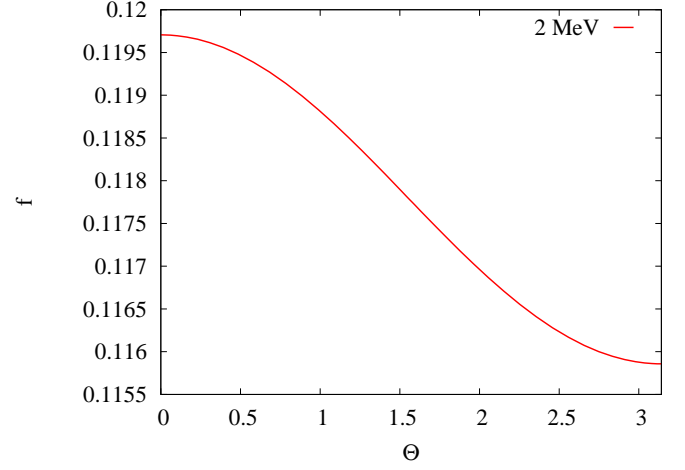


Fig. 11. 2 MeV averaged neutrino distribution function as a function of Θ at $r = R_*$ at time $t = T$

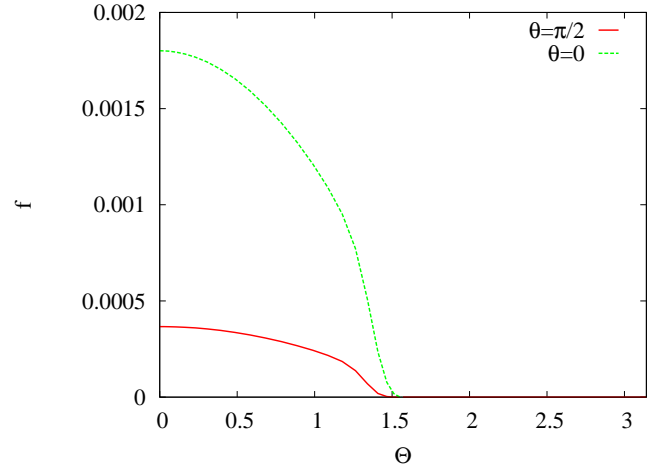


Fig. 12. 2 MeV averaged neutrino distribution function as a function of Θ at the surface of the star

is computed. Remember that spectral methods lose their efficiency when discontinuities appear. In order to overcome this difficulty we propose the adoption the method used in computing the steady state configuration of a fast rotating star.

We make a coordinate transformation

$$r' = r + r^3 f(\theta), \quad (53)$$

where $f(\theta)$ determines the surface of the star. The Liouville operator \mathcal{L}_{sph} is slightly modified but there is no change in the outlined procedure.

The problem is that the plasma is not at rest and violates the validity of the hypothesis we have taken. To overcome this difficulty we propose a reference frame transformation using a coordinate transformation

$$\phi' = \phi + \Omega t. \quad (54)$$

In this comoving frame, the matter is at the rest. We have to solve the transfer equation modified by the metric terms generated by the rotation (see e.g. Debbasch & van Leeuwen (2009) for a derivation of the equation with the metric terms taken into account).

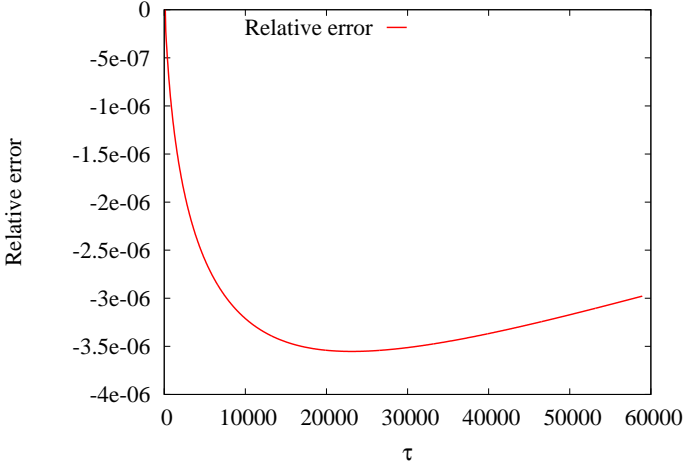


Fig. 13. 2 MeV Relative error on conservation number of neutrino.

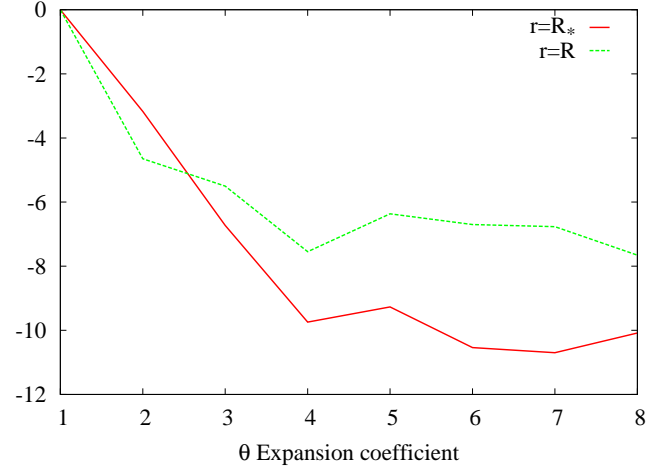


Fig. 15. 2 MeV logarithm of averaged amplitude of θ coefficients expansion divided by the first coefficient, at $r = R_*$ (lower plot) and at $r = R$ (upper plot)

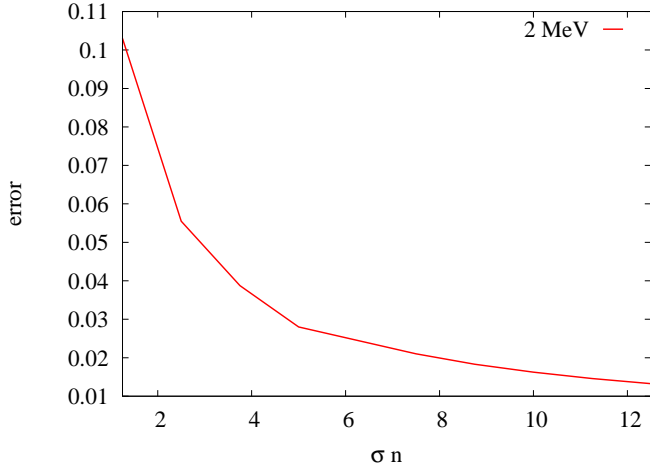


Fig. 14. 2 MeV matching relative error. (See text)

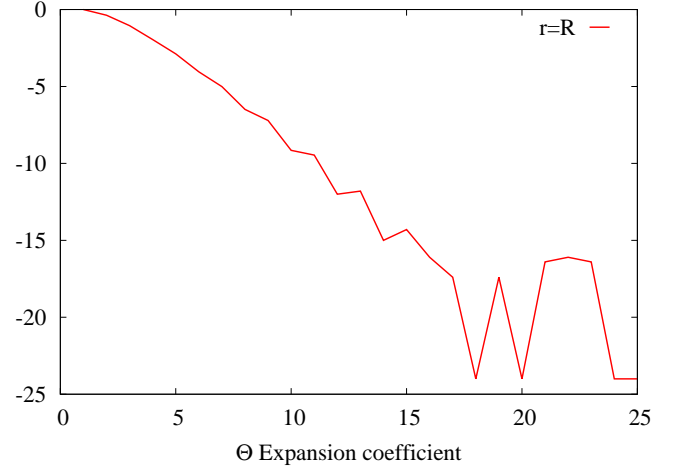


Fig. 16. 2 MeV logarithm of averaged amplitude of Θ Tchebitchev expansion coefficients, divided by the first coefficient, at $r = R$

We conclude this section by describing a strategy to compute the cooling of a neutron star. The numerical problem lies in the presence of two characteristic times, τ_1 and τ_2 . τ_1 is the neutrino propagation time within the star (of the order of a few milliseconds, see Fig 6). The second one τ_2 is the characteristic time given by the heat capacity of the star and the energy flux. τ_2 is of the order of years. In order to overcome this difficulty, we proceed with a two times technique.

Consider a NS at time $t = 0$ with a null neutrino distribution. Let $T(r, 0)$ be its temperature profile. By tacking the density and temperature profile fixed, let the neutrino density $F(r, \theta, \Phi, t)$ relax towards a steady state regime. (Of course the neutrino emission and absorption coefficients are taken into account). The first step can be time consuming, if the initial neutrino distribution is far from the steady state one. Once a steady state regime is reached, by using the neutrino flux we can compute the new temperature distribution of the star, the flux being considered frozen. With the new frozen temperature we re-compute the new neutrino distribution. The number of time steps required to reach the new steady sate neutrino distribution function is much shorter than the previous one because we start from a distribution close to the relaxed one.

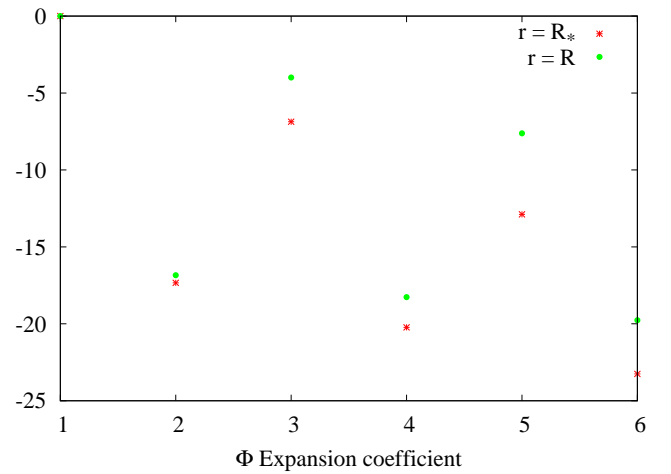


Fig. 17. 2 MeV logarithm of averaged amplitude of Φ Fourier expansion coefficients divided by the first coefficient at $r = R_*$ (lower plot) and at $r = R$

7. Conclusion

The aim of this numerical work was to assess a “proof of principle” for the treatment of the full transport equation in 6D spherical coordinates in a single core processor, in reasonable physical and computational situations, and by means of the use of spectral methods in phase space. We emphasize the fact that as far as we know, a 6-dimensional approach in spherical-like coordinates has never been attempted before, and that consequently no comparison with existing works can be made. A particular setting of the computational grid is necessary for treating singular behaviour of some terms in the Liouville operator. Meaningful numerical results are obtained in a very reasonable computational time, the most time consuming operation being the computation of the Liouville operator. For problems where Fokker-Planck-like approximations can not be used, it is possible that the most consuming computation would be related to the collision term, in which the thermal distribution of the plasma has to be taken in to account. (See Eq.(14)). We believe that spectral methods are suited to build an efficient algorithm for the treatment this problem. We have also seen that the use of a fully spectral scheme in treating the advection term can turn out to be useful if reduction of the CPU time is a priority. We believe that by using fairly reasonable parallel computation on a small-scale cluster, one would be able to perform multiple runs in physically relevant 6-dimensional settings and in a really quick fashion. Although we are aware of the fact that several ingredients are still to be added to the transport description to use it in a physically relevant radiation hydrodynamics code, our results support the fact that no fundamental technical difficulty should arise in tackling those issues.

Acknowledgements. We wish to thank Ericourgoulhon, Jérôme Novak and Micaela Oertel for the many fruitful discussions during the development of this method. N.V. acknowledges the support of the Swiss National Science Foundation under the grant No PP002-106627/1, and of the French ANR Grant 06-2-134423 entitled “Méthodes mathématiques pour la relativité générale”. B.P. acknowledges the support of the SN2NS project ANR-10-BLAN-0503.

References

- Anderson, J. L. & Spiegel, E. A. 1972, ApJ, 171, 127
 Bonazzola, S., Gourgoulhon, E., & Marck, J.-A. 1999, Journal of Computational and Applied Mathematics, 109, 433
 Bonazzola, S. & Marck, J.-A. 1990, Journal of Computational Physics, 87, 201
 Bruenn, S. W. 1985, Astrophys. J. Suppl., 58, 771
 Canuto, C., Hussaini, M. Y., Quarteroni, A., & Zang, T. A. 1988, Spectral methods in fluid dynamics (Springer Verlag)
 Canuto, C., Hussaini, M. Y., Quarteroni, A., & Zang, T. A. 2006, Spectral methods: fundamentals in single domains (Springer Verlag)
 Cardall, C. & Mezzacappa, A. 2003, Phys. Rev. D, 68, 023006
 Debbasch, F. & van Leeuwen, W. A. 2009, Physica A Statistical Mechanics and its Applications, 388, 1079
 Gottlieb, D. & Orszag, S. 1977, Numerical analysis of spectral methods: theory and applications (SIAM)
 Gourgoulhon, E. & Haensel, P. 1993, A&A, 271, 187
 Grandclement, P. & Novak, J. 2009, Liv. Rev. Rel., Irr-2009-1
 Janka, H.-T., Langanke, K., Marek, A., Martínez-Pinedo, G., & Müller, B. 2007, Phys. Rep., 442, 38
 Kompaneet, A.-S. 1957, Soviet Phys.-JETP Lett., 4, 730
 Leveque, R. J. 2002, Finite Volume methods for hyperbolic problems (Cambridge University press)
 Levermore, C. D. 1979, report No. UCID-18229, Lawrence Livermore national laboratory
 Liebendörfer, M., Rampp, M., Janka, H.-T., & Mezzacappa, A. 2005, ApJ, 620, 840
 Liebendörfer, M., Whitehouse, S. C., & Fischer, T. 2009, ApJ, 698, 1174
 Marek, A. & Janka, H.-T. 2009, ApJ, 694, 664
 Messer, O. E. B., Bruenn, S. W., Blondin, J. M., Hix, W. R., & Mezzacappa, A. 2008, Journal of Physics Conference Series, 125, 012010
 Mezzacappa, A. & Matzner, R. A. 1989, ApJ, 343, 853

- Müller, B., Janka, H.-T., & Dimmelmeier, H. 2010, ApJS, 189, 104
 Pomraning, G. C. 1973, The equations of radiation hydrodynamics (Dover)
 Thorne, K. S. 1981, MNRAS, 194, 439

Appendix A: Particle conservation in the transport equation

We will concentrate here on the pure coherent scattering case of transport equation for photons, which writes:

$$\frac{1}{c} \frac{\partial F}{\partial t} + \mathcal{L}_{sph} F + \sigma_t F - \int_{4\pi} \sigma_d(\omega \cdot \omega') \sin \Theta' d\Phi' = 0. \quad (A.1)$$

The above equation can be written, after multiplication by the element volume of the space of phase $r^2 \sin \theta \sin \Theta$ as

$$\frac{1}{c} \frac{\partial}{\partial t} (Fr^2 \sin \theta \sin \Theta) + \frac{\partial}{\partial r} (Fr^2 \sin \theta \sin \Theta \cos \Theta) \quad (A.2)$$

$$+ \frac{\partial}{\partial \theta} (Fr \sin^2 \Theta \sin \theta \cos \Phi) - \frac{\partial}{\partial \Theta} (Fr \sin^2 \Theta \sin \theta) \quad (A.3)$$

$$+ \frac{\partial}{\partial \phi} (Fr \sin^2 \Theta \sin \Phi) - \frac{\partial}{\partial \Phi} (Fr \sin^2 \Theta \cos \theta \sin \Phi) \quad (A.4)$$

$$+ r^2 \sin \Theta \sin \theta \left(\sigma_t F - \int_{4\pi} \sigma_d(\omega \cdot \omega') F \sin \Theta' d\Theta' d\Phi' \right) = 0. \quad (A.5)$$

After an integration on $r, \theta, \phi, \Theta, \Phi$, and provided the detailed balance condition (Pomraning 1973)

$$\sigma_d(\gamma' \rightarrow \gamma, \omega' \rightarrow \omega) = \sigma_d(\gamma \rightarrow \gamma', \omega \rightarrow \omega') \quad (A.6)$$

holds, we obtain

$$\frac{\partial N}{\partial t} + J_{R_2} - J_{R_1} = 0, \quad (A.7)$$

where

$$N = \int_{R_1}^{R_2} r^2 dr \int_{4\pi} \sin \theta d\theta d\phi \int_{4\pi} \sin \Theta d\Theta F \quad (A.8)$$

is the number of particles and

$$J_{R_2} = R_2^2 \int_{4\pi} \sin \theta d\theta d\phi \times \int_{4\pi} \sin \Theta \cos \Theta d\Theta d\Phi F(t, R_2, \theta, \phi, \Theta, \Phi) \quad (A.9)$$

is the flux of ingoing (outgoing) particles into the surface $r = R_2$ of the spherical shell $R_1 \leq r \leq R_2$. The same definition holds for J_{R_1} with respect to the radius R_1 . This is a conservative form of the transport equation (A.1).

In the general case when energy dependence is taken in to account, the photon number conservation is obtained after integration on the energy $\gamma = hv/mc$. If induced scattering processes are also considered, The conservation equation Eq (A.7) is obtained thanks to the detailed balance condition (A.6).

Appendix B: Enhanced spectral treatment in 2-D case: The conservative formulation

We present a spherically symmetric version of an algorithm for a spectral treatment, amounting to the 2-D case $F(r, \Theta, t)$ for the distribution function, and restricted to coherent Thompson scattering interactions. This approach is useful to show how the a prospective full spectral treatment should be handled, and how its inherent difficulties can be overcome. As opposed to what we did previously, we shall now use the conservative form explicated in Eq.(A.2)) for the numerical representation of the distribution function: We introduce the new function (see Appendix A)

$$\hat{F}(r, \Theta, t) = r^2 \sin \Theta F(r, \Theta, t) \quad (\text{B.1})$$

Using the previously defined value for the total Thompson cross section σ^{Tot} in photon scattering, the 2-D conservative form of the transfer equation reads, after integration on the Φ angle¹⁰:

$$\begin{aligned} \frac{\partial \hat{F}}{\partial t} + \cos \Theta \frac{\partial \hat{F}}{\partial r} - \frac{1}{r} \left(\sin \Theta \frac{\partial \hat{F}}{\partial \Theta} + \cos \Theta \hat{F} \right) \\ = n(r) \sigma^{Tot} \times \left[-\hat{F}(r, \Theta, t) + \frac{3}{8} \sin \Theta \int_0^\pi \left(1 + (\cos \Theta \cos \Theta')^2 + \frac{1}{2} (\sin \Theta \sin \Theta')^2 \right) \hat{F}(r, \Theta', t) d\Theta' \right] \end{aligned} \quad (\text{B.2})$$

We shall consider the same boundary problem that the one presented in the 5-D hybrid case, namely $\hat{F}(r, \Theta, t = 0) = 0$ as initial value, $\hat{F}(R_1, \Theta, t) = \cos \Theta \sin \Theta$ for $0 \leq \Theta \leq \pi/2$ and $\hat{F}(R_2, \Theta, t)$ for $\pi/2 \leq \Theta \leq \pi$. The time evolution will lead to a discontinuous solution in the radial direction. Spectral methods are not suited to handle this kind of problem. In order to show that, consider the simple advection equation

$$\frac{\partial \Phi}{\partial t} + C \frac{\partial \Phi}{\partial r} = 0, \quad (\text{B.3})$$

where $C > 0$ is a constant and $R_1 \leq r \leq R_2$, with the initial data $\Phi(r, 0) = 0$ and the boundary condition $\Phi(R_1, t) = 1$. This problem is clearly analogous to ours, although simpler; it is also well known that the solution is an Heaviside function $\Phi(r, t) = \Theta(r - Ct)$ propagating in our setting from the inner radius R_1 to the outer radius R_2 at velocity C . We expect to obtain a solution to our problem with similar properties. As we have already said, spectral methods are in general not well suited to treat discontinuous solutions, except if some algorithm is used to smear out the solution (Gottlieb & Orszag 1977). In particular, it is possible to introduce viscosity in the spectral scheme, which can be partly treated in the coefficient space (Bonazzola & Marck 1990). However, such a scheme would have severe effects on conservation laws in our case. In what follows, we shall show an algorithm which attempts to overcome such difficulties.

A classical first order implicit time discretisation to the simple advection problem above (the so-called Euler method) leads to

$$\Phi^{j+1}(r) = \Phi^j(r) - C \Delta t \frac{\partial \Phi^{j+1}}{\partial r}, \quad (\text{B.4})$$

¹⁰ This formulation allows to us to check the conservation law term by term: After an angular integration on Θ , the right-hand side and the second term on the left-hand side of the Eq.(B.2) vanish. The integrated first term on the left expresses then exactly the balance in radial flux.

where Φ^j is the value of the solution at time $t = j\Delta t$. and Δt is elementary time interval. We solve the above equation by making an expansion in Chebyshev polynomials, imposing boundary values using a classical Tau approach (Gottlieb & Orszag 1977) and with different values of the parameter Δt .¹¹

Fig. B.1. shows the numerical and analytical solutions obtained with $N_r = 65$ points in the propagation direction and $\Delta t = 3(R_2 - R_1)/(CN_r^2)$ (this corresponds to 3 times the maximal value satisfying the stability Courant condition for an *explicit* numerical scheme). As expected, we observe strong oscillations in the solution due to the Gibbs phenomenon occurring at the solution discontinuity. Note that the propagation velocity for the solution seems however to be empirically correct.

Numerical and analytical solutions using the much bigger value $\Delta t = 24(R_2 - R_1)/(CN_r^2)$ are displayed in Fig. B.1. While oscillations have disappeared, the numerical solution is spread out (the numerical propagation velocity being still correct). We have found experimentally that a value of about

$$\Delta t_{opt} = \frac{8}{CN_r^2} (R_2 - R_1) \quad (\text{B.5})$$

gives the best results, as shown in Fig. B.1. The above value seems quite independent on the number of spectral radial points: It holds for $17 \leq N_r \leq 257$ in this particular problem. On the contrary, we have observed that a second order scheme of the type:

$$\Phi^{j+1} + \frac{C\Delta t}{2} \frac{\partial \Phi^{j+1}}{\partial r} = \Phi^j - \frac{C\Delta t}{2} \frac{\partial \Phi^j}{\partial r} \quad (\text{B.6})$$

leads to an incorrect propagation velocity.

In order to compare the results obtained with the first order finite difference scheme and the spectral one, we plot the values for the derivative $\partial_r \Phi$ (see Fig. B.1. We recover similar results for the amplitude of derivatives when the grid point number ratio between the finite differences scheme and the spectral one is about five (330 points versus 65). The size ratio mentioned in the introduction seems then to be verified. Finally, Fig. B.2 shows the error on the conservation of particles for this scheme, namely the verification of the identity:

$$\frac{\partial}{\partial t} \int_{R_1}^{R_2} \Phi(r, t) dr + C (\Phi(R_1, t) - \Phi(R_2, t)) = 0. \quad (\text{B.7})$$

The above simple and fast algorithm seems indeed to be able to handle correctly the discontinuities in the solution, keeping conservative features at the same time. It is tempting to apply it in solving the Eq.(B.2). Let us write this equation in the following effective way:

$$\hat{F}_k^{j+1} - \cos \Theta_k \frac{\partial \hat{F}_k^{j+1}}{\partial r} \Delta t = \hat{F}_k^j + \Delta t S_k^{j+1/2} \quad (\text{B.8})$$

where $\hat{F}_k^j = \hat{F}(r, \Theta_k, t_j)$, Θ_k is the value of the discretised variable Θ , and S_k contains all differential terms on \hat{F} , taken on the same values, appearing in Eq. (B.2). The coefficient in front of $\partial_r \hat{F}$ depends on the variable Θ . As a consequence, we cannot *a priori* define a consistent optimal value Δt_{opt} for every value of Θ as in Eq.(B.5). Moreover, we want to be free in choosing the value of Δt , which will in general be constrained by a Courant stability

¹¹ The matrix of differential operator in the Chebyshev basis can be reduced easily thanks a linear combination of the lines, to a tridiagonal matrix. This leads to a considerable speedup of the algorithm.

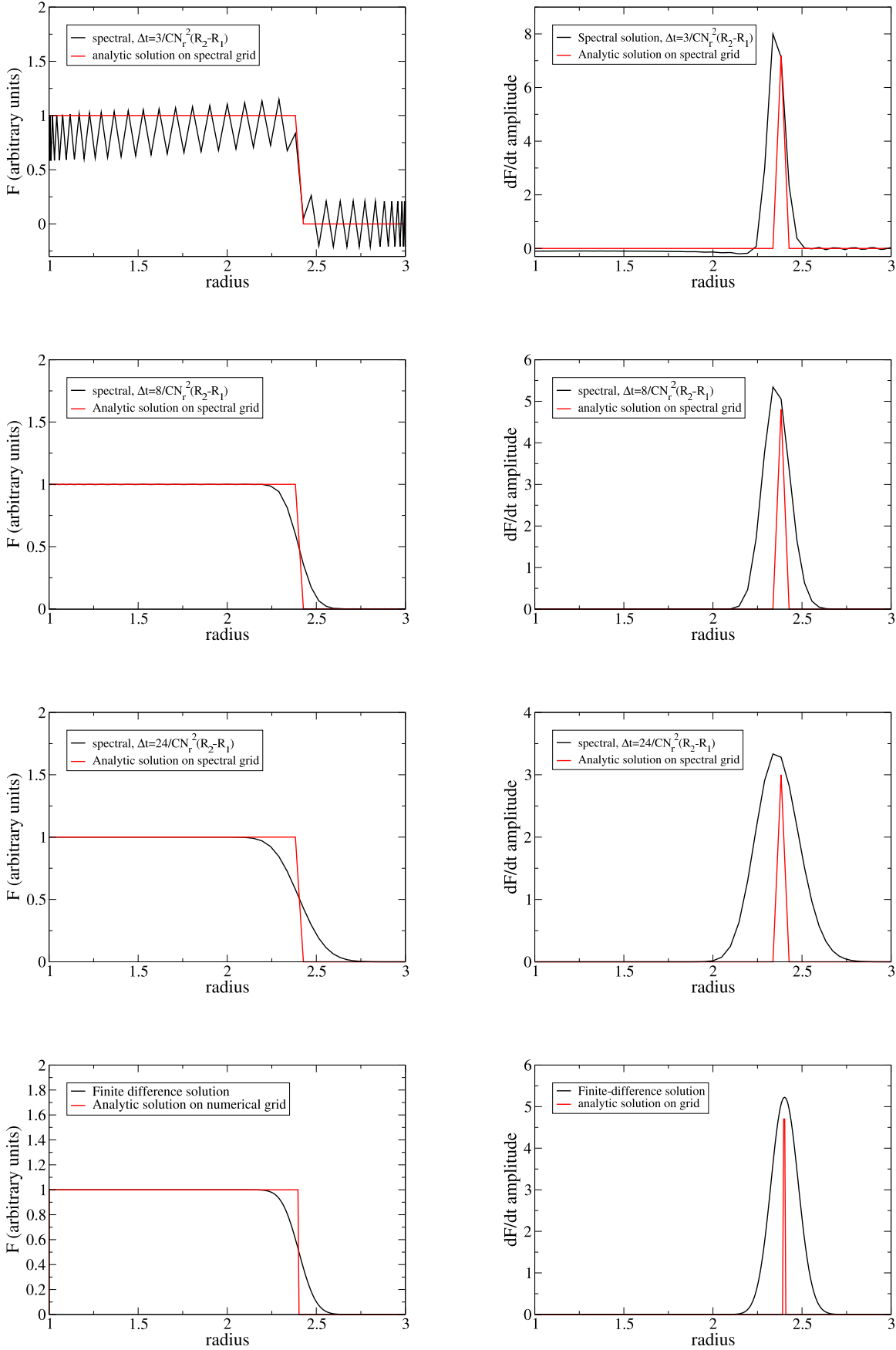


Fig. B.1. Resolution of the advection problem for a shock profile using spectral methods. The left panels show the radial profile for different choices of the time step, along with the analytical solution (interpolated to the spectral grid) and a finite-difference solution (lower left panel). In the spectral solver, the number of grid points is $N_r = 65$, whereas in the finite-difference solver, the choice $N_r = 325$ is made. The right panel shows a comparison for the values of the function derivative in the spectral cases and the finite difference one. The amplitude of the derivative is a good indicator of the diffusivity of the numerical scheme. Note that the derivative of spectral solution is larger than the one of the finite difference scheme. The value $C=1$ is here chosen.

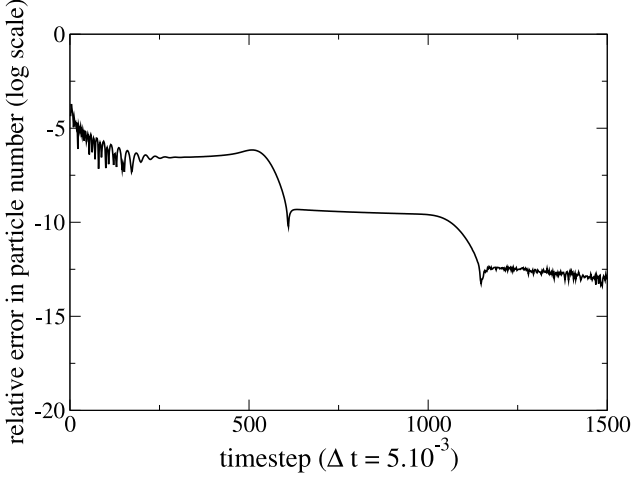


Fig. B.2. Relative variation of particle number at a given time step,

condition, either related to the transport equation itself or an adjacent hydrodynamic scheme. We proceed then in the following way: consider first an time explicit version of Eq. (B.8):

$$\hat{F}_k^{j+1} = \hat{F}_k^j + \cos \Theta_k \frac{\partial \hat{F}_k^j}{\partial r} \Delta t + \Delta t S_k^j. \quad (\text{B.9})$$

This can be viewed as a set of N_Θ equations, where terms are evaluated for each value of the discretized angle Θ_k . We define for each of those angles an optimal time step:

$$\Delta t_{opt}^k = \frac{8}{\cos(\Theta_k) N_r^2} (R_2 - R_1). \quad (\text{B.10})$$

If $\Delta t_{opt}^k \geq \Delta t$, we compute the variation

$$G_k^j(t) = \hat{F}_k(t_j + \Delta t_{opt}^k) - \hat{F}_k(t_j) = \Delta t_{opt}^k \cos \Theta_k \frac{\partial \hat{F}_k(t_j)}{\partial r}. \quad (\text{B.11})$$

A simple linear interpolation is then performed to obtain the updated value for \hat{F}_k^{j+1} :

$$\hat{F}(r, \Theta_k, t_j + \Delta t) = \hat{F}_k^{j+1} = \hat{F}_k^j + G_k^j \cos \Theta_k \frac{\Delta t}{\Delta t_{opt}^k} + \Delta t S_k^j. \quad (\text{B.12})$$

The case $\Delta t > \Delta t_{opt}$ is treated by introducing an intermediate time interval

$$t_{int}^k = \Delta t / K \leq \Delta t_{opt}^k, \quad (\text{B.13})$$

where K is the smallest integer satisfying the above relation, and performing the numerical integration K times per global time step.

In the implicit setting of Eq. (B.8) and with $\Delta t_{opt}^k \geq \Delta t$, we slightly correct the previous scheme by defining:

$$G_{k,\epsilon}^j(t_j) = \Delta t_{opt}^k \cos \Theta_k \frac{\partial \hat{F}_k(t_j)}{\partial r} + \epsilon (\Delta t_{opt}^k)^2, \quad (\text{B.14})$$

where the real parameter ϵ is tuned in the algorithm so that the partial update

$$\hat{F}_k^{j+1*} = \hat{F}_k^j + G_{k,\epsilon}^j \cos \Theta_k \frac{\Delta t}{\Delta t_{opt}^k} \quad (\text{B.15})$$

satisfies exactly a radial flux balance for particle number. The update is completed by the implicit first-order step

$$\hat{F}_k^{j+1} = \hat{F}_k^{j+1*} + \Delta t S_k^{j+1}. \quad (\text{B.16})$$

The case $\Delta t > \Delta t_{opt}$ is also performed by splitting time updates as in Eq. (B.13).

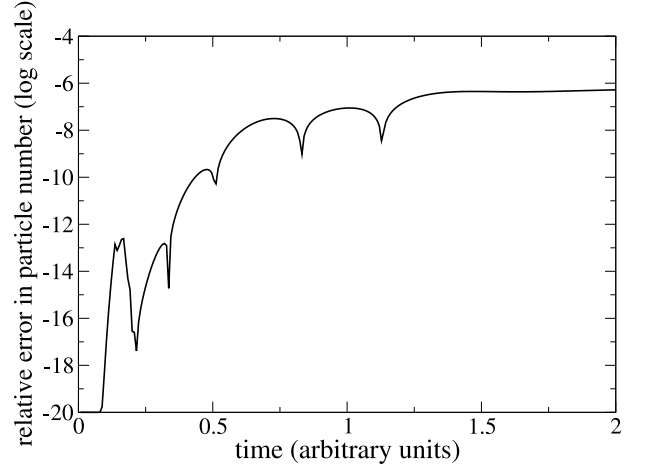


Fig. B.3. Relative variation of particle number at a given time step, for the hybrid resolution of the 2D transport equation (B.2). The number of spectral points is $N_r = 65$, with two finite difference zones of 30 radial grid points at the edges. The error is mainly due to the differential term on Θ . It decreases exponentially when the number of grid points in Θ increases.

In solving the Eq.(B.2) in the domain represented in Fig. 2, strong oscillations due to discontinuities may appear near the edges of the interval, if the plasma density there does not vanish (see Sect. 5.2 and Fig. 6). A spectral resolution is in principle not able to handle these oscillations. To overcome this problem, We have split the interval in 3 sub-intervals, two of them being close to the radial edges of the main interval, and each outer sub-interval having a width of 0.1 of the main interval. The solution in the sub intervals is computed with a finite difference scheme, using 30 grid points. The solution in the largest central interval is computed with the spectral scheme presented just above, using 65 spectral points and again performing an expansion on a Chebychev polynomial basis. A Chebychev polynomial expansion is also, as before, used to treat the Θ dependence.

Results on Fig. B.3 show the conservation of the number of particles using this approach, with the settings of Sect. 5.2. This shows the validity of our scheme in the bulk and at domain boundaries, and the accuracy of the conservative formulation in this 2D example.

Once known $\hat{F} = r^2 \sin \Theta F$, the distribution function F is recovered easily by manipulating the coefficients in the spectral decomposition; the division by $\sin \Theta$ is nicely handled in the coefficient space, whereas the division by r is performed in the configuration space.

In this test, 25 points are used in the Θ direction, and $(30 + 25 + 30)$ points in the radial direction for finite difference and spectral zones. The only Courant constraint for the timestep in the radial direction comes from the finite-difference zones, as an

implicit spectral resolution in the radial direction is performed in the central domain. The timestep used is then $\Delta_t = 5 \times 10^{-3}$.

In conclusion, treating the transport equation with a fully spectral code is not straightforward. In the above (hybrid) example in the radial direction, the simulation requires a total of 125 grid points in r . As shown previously, in order to obtain the same accuracy with a first order finite scheme, a rough number of 330 grid points would be necessary. This leads to a size ratio of 2.64, two times less than previously expected.

It is possible that the advantage of a spectral scheme reduces with more sophisticated higher order finite differences schemes. However, to match the performances of the presented approach, such a scheme should be of order 2 or more, exhibit weak diffusivity and show no oscillations due to discontinuities.

Appendix C: The two moments approximation: Diffusion and telegraph equation

The two moments approximation consists of making a spherical harmonics expansion in Θ and Φ and neglecting all the moments higher than one. We obtain the well known diffusion equation and the telegraph equation that can turn out to be interesting in the case of fast time variability of the matter density.

Let us write the transfer equation for neutrinos in the general form

$$\begin{aligned} \frac{1}{c} \frac{\partial F}{\partial t} + \nabla F \cdot \omega + n(r, \theta, \phi) + \\ [4\pi F(r, \theta, \phi, \Theta, \Phi, t) \\ - \int_0^{2\pi} d\Phi' \int_0^\pi (a + b \omega \cdot \omega') F(r, \theta, \phi, \Theta', \Phi', t) \sin \Theta' d\Theta'] \\ = S(r, \theta, \phi, t), \end{aligned} \quad (\text{C.1})$$

where $a(E) + b(E) \omega \cdot \omega'$ is the differential neutrino nucleon cross section σ_D , $n(r, \theta, \phi)$ is the baryonic density, and $S(r, \theta, \phi, t)$ contains the source terms. We consider only the two first moments:

$$F(r, \theta, \phi, \Theta, \Phi, t) = F^0(r, \theta, \phi, t) + 3 \mathbf{F}^1(r, \theta, \phi, t) \cdot \omega. \quad (\text{C.2})$$

By averaging over Θ and Φ : $1/4\pi \int_\Omega d\Omega$ we obtain

$$\frac{1}{c} \frac{\partial F^0}{\partial t} + \nabla \cdot \mathbf{F}^1 = S. \quad (\text{C.3})$$

After multiplying $F(r, \theta, \Theta, \Phi, t)$ by ω , averaging over the solid angle gives

$$\frac{1}{c} \frac{\partial \mathbf{F}^1}{\partial t} + \frac{1}{3} \nabla F^0 + \tilde{\tau} \mathbf{F}^1 = 0, \quad (\text{C.4})$$

where $\tilde{\tau}$ is the optical depth

$$\tilde{\tau} = 4\pi \left(a(E) - \frac{1}{3} b(E) \right) n(r, \theta, \phi, t). \quad (\text{C.5})$$

The *Eddington* (or diffusion) approximation consists in neglecting the time derivative in Eq.(C.4). In this case we have the Fick law

$$\mathbf{F}^1 = -\frac{1}{3n\tilde{\tau}} \nabla F^0, \quad (\text{C.6})$$

and the diffusion equation reads

$$\frac{1}{c} \frac{\partial F^0}{\partial t} - \nabla_j \left(\frac{1}{3\tilde{\tau}} \nabla^j F^0 \right) = S. \quad (\text{C.7})$$

We propose to go further with the approximation. To do this, take the time derivative of Eq.(C.3)

$$\frac{1}{c^2} \frac{\partial^2 F^0}{\partial t^2} + \frac{1}{c} \frac{\partial \nabla_j F^{1j}}{\partial t} = \frac{1}{c} \frac{\partial S}{\partial t}, \quad (\text{C.8})$$

and take the divergence of Eq.(C.4)

$$\frac{1}{c} \frac{\partial \nabla_j F^{1j}}{\partial t} + \frac{1}{3} \left(\Delta F^0 + (\nabla_j \tilde{\tau}) F^{1j} + \tilde{\tau} \nabla_j F^{1j} \right) = 0. \quad (\text{C.9})$$

By replacing $\partial \nabla_j F^{1j} / \partial t$ in Eq.(C.8) we obtain

$$\frac{1}{c^2} \frac{\partial^2 F^0}{\partial t^2} - \frac{1}{3} \left(\Delta F^0 + (\nabla_j \tilde{\tau}) F^{1j} + \tilde{\tau} \nabla_j F^{1j} \right) = \frac{1}{c} \frac{\partial S}{\partial t}. \quad (\text{C.10})$$

In the above equation the term $\nabla_j F^{1j}$ comes from the one obtained in Eq.(C.3) and $(\nabla_j \tilde{\tau}) F^{1j}$ comes from Eq.(C.4) in which the time derivative is neglected. In the end, we obtain the following telegraph equation

$$\frac{1}{\tilde{\tau}} \left(\frac{3}{c^2} \frac{\partial^2 F^0}{\partial t^2} - \Delta F^0 \right) + \frac{1}{c} \frac{\partial F^0}{\partial t} - \nabla_j \left(\frac{1}{\tilde{\tau}} \right) \nabla^j F^0 = S + \frac{1}{c\tilde{\tau}} \frac{\partial S}{\partial t}. \quad (\text{C.11})$$

When the time variations are weak, we recover the diffusion equation, Eq.(C.7). The propagation velocity of the signal is $\leq c/\sqrt{3}$ which is more satisfactory, in a relativistic context, especially when the matter motion is close to the velocity of the light, than the diffusion equation which gives an infinite propagation velocity. Note that if $\tilde{\tau}$ is constant the result is exact.